

Electron-impact excitation and emission cross sections of the H₂ Lyman and Werner Systems

Xianming Liu and D. E. Shemansky

Department of Aerospace Engineering, University of Southern California, Los Angeles

Syed M. Ahmed

Institute for Plasma Research, Gandhinagar, India

G. K. James and J. M. Ajello

Jet Propulsion Laboratory, California Institute of Technology, Pasadena

Abstract. Excitation functions of the H₂ Lyman (Ly) ($B\ ^1\Sigma_u^+ - X\ ^1\Sigma_g^+$) and Werner (W) ($C\ ^1\Pi_u - X\ ^1\Sigma_g^+$) band systems have been reanalyzed using a combination of measurements and theoretical considerations. These systems are prominent emitters in outer planet atmospheric dayglow and auroral activity and can be used to infer energy deposition and heating rates. Earlier measurements of the cross sections reported by *Shemansky et al.* [1985a] have been found to be inaccurate in the threshold energy region. A combination of high-resolution spectral and shape function measurements obtained at the Jet Propulsion Laboratory (JPL) in low- and medium-energy regions have been used to obtain relative excitation shape functions of the two systems. At energies above 250 eV, we have used the measurements obtained earlier by *De Heer and Carrière* [1971] in order to define the first two terms of the Born electric dipole collision strength. The complete set of collision strength terms is obtained by combining the JPL and *De Heer and Carrière* [1971] data. We have found that, contrary to results of *Shemansky et al.* [1985a], the shape functions of the H₂ Ly and W systems, expressed in units of threshold energy, are the same within experimental error. Absolute cross sections of the H₂ Ly and W systems are established using the theoretical oscillator strengths of *Abgrall et al.* [1987, 1993a, b, c] and *Abgrall and Roueff* [1989]. The atomic hydrogen H Ly α emission cross section resulting from dissociative excitation of H₂ at 100 eV obtained from relative intensities of H₂ W emission lines is also derived and compared with other experimental measurements. At a gas temperature of 300 K and electron energy of 100 eV, the cross sections for the H Ly α , H₂ Ly, and W emissions are $(0.716 \pm 0.095) \times 10^{-17}$, $(2.62 \pm 0.34) \times 10^{-17}$, and $(2.41 \pm 0.31) \times 10^{-17} \text{ cm}^2$, respectively. The accuracy of the absolute values and shape functions is limited primarily by electron gun performance, as was the case for *Shemansky et al.* The rotational dependence of the transition dipole matrix elements and perturbations between the $B\ ^1\Sigma_u^+$ and $C\ ^1\Pi_u^+$ states have a significant effect on the cross sections.

1. Introduction

Electron impact excitation of molecular hydrogen is the primary excitation mechanism in molecular clouds and atmospheres of the outer planets. Accurate excitation cross sections in the near-threshold region are essential for the determination of excitation conditions. The dayglow and auroral activity in the outer planet at-

mospheres produce emission characteristic of low-energy electron impact [Pryor et al., 1998; Ajello et al., 1998], and diagnostics of excitation processes depend on accurate cross sections. Accurate excitation cross sections are also important for plasma science [Fujimoto and Sawada, 1995] and a prerequisite for modeling swarm and plasma etching, understanding hydrogen gas lasers, and for optimizing hydrogen anion sources [Hiskes et al., 1985; Hiskes, 1992, 1994, 1996].

The most extensively studied and referenced H₂ Lyman (Ly) and Werner (W) cross sections in earlier publications are those of *Shemansky et al.* [1985a] (hereafter referred to as SAH). Subsequently, we have found

Copyright 1998 by the American Geophysical Union.

Paper number 98JA02721.

0148-0227/98/98JA-02721\$09.00

that instabilities in the electron gun system caused serious errors in shape function measurement. The experimental problems have been only partially corrected at the Jet Propulsion Laboratory (JPL) facility. We have found it is necessary to utilize several techniques to establish satisfactorily accurate cross sections. First, a high-resolution 3-m spectrometer in tandem with a collision chamber has been used to measure the excitation shape function in the 13.5–1200 eV region (use of this data, however, is limited to below 250 eV). Second, high-resolution measurements of the H₂ spectra at selected excitation energies are utilized to establish the relative shape function of the H₂ Ly and W systems. The measurements of the W system shape function by *De Heer and Carrière* [1971] at higher energies are judged to be the most accurate among the available data and are used to characterize the shape function in the region above 100 eV. Excitation functions and cross sections obtained from merging the present and *De Heer and Carrière* [1971] measurements are established on an absolute scale with accurate optical absorption oscillator strengths calculated by *Abgrall et al.* [1987, 1993a, b, c] and *Abgrall and Roueff* [1989]. The effects of the perturbations between B¹Σ_u⁺ and C¹Π_u states and *J* dependence of the transition dipole matrix elements are fully taken into account.

We find that the earlier results of SAH were limited by low spectral resolution and instability of the electron gun. An examination of the electron gun parameters revealed an intrinsic instability in performance, indicating that a new design is required if reliable results are to be obtained. The most serious error in the SAH result is in the relative cross sections at low energies. The ratio of the cross sections, Ly/W, is abnormally large at low energies in the SAH result. For example, the SAH Ly/W cross-section ratio at 20 eV is 5.4, while the ratio obtained by *Khakoo and Trajmar* [1986] is only 1.4.

This paper is arranged in six sections. Section 2 describes new experimental measurements. Three experimental studies are performed. (1) Excitation functions of the H₂ Ly and W bands are measured in the low- and medium-energy regions. (2) The relative intensities of a group of emission lines are measured and modeled to determine the relative shape functions of the two systems. (3) The H Ly α emission cross section from dissociative excitation of H₂ is derived from the absolute C¹Π_u state cross section at 100 eV. Experimental difficulties with the stability of magnetically collimated electron guns are also discussed. Section 3 reviews the theoretical model utilized to obtain excitation functions and cross sections from experimental measurements. Section 4 discusses the energy calibration, background subtraction, and data analysis. Section 5 presents the measured H₂ Ly and W excitation cross sections compared to earlier excitation cross sections. The effect of the ¹Σ_u⁺–¹Π_u⁺ coupling, rotational dependence of transition dipole matrix elements, and temperature dependence of the cross sections are discussed. Section 6 summarizes the results.

Excitation functions and cross sections presented in this paper do not include resonance and cascade effects. Cross sections for these additional processes will be addressed in later publications.

2. Experiment

2.1. Measurement of the B¹Σ_u⁺ and C¹Π_u State Excitation Functions

The experimental setup at JPL has been described in detail elsewhere [Liu et al., 1995]. The system consists of a 3-m vacuum ultraviolet spectrometer (Acton VM-523-SG) and an electron collision chamber. Electrons generated by heating a thoriated tungsten filament are collimated with an axially symmetric magnetic field of ~100 G and accelerated to energies in the range from few eV to ~2000 eV with energy resolution of ~0.5 eV. The accelerated electrons collide with uniform hydrogen gas (1×10^{-4} ~ 5×10^{-6} torr). Optical emission from electron impact excited H₂ was dispersed with the 3-m spectrometer equipped with a 1200 groove/mm grating coated with Al+MgF₂ and was detected with a channel electron multiplier (Galileo 4503) coated with CsI. A Faraday cup was used to minimize backscattered electrons and monitor the electron beam current.

Electron-impact excitation of H₂ can take place by direct (electric dipole) and indirect excitation mechanisms. Direct excitation involves electronic transitions between the X¹Σ_g⁺ and the B¹Σ_u⁺ and C¹Π_u states, while indirect excitation involves other intermediate states and species. In the low-energy region, Feshbach resonance and cascade excitations are prominent. Resonance excitation arises from the capture of a slow electron by H₂ to form molecular H₂⁻, decaying rapidly to H₂ in the B¹Σ_u⁺ and C¹Π_u states. The contribution of resonance excitation is substantial in the threshold energy region but negligibly small as the excitation energy increases above 15–16 eV. Cascade excitation of the B¹Σ_u⁺ and C¹Π_u states generally takes place by dipole-forbidden excitation from the X¹Σ_g⁺ state to the EF, GK, and HH¹Σ_g⁺ states, followed by cascade to the singlet u states. Since cascade primarily occurs between the E, F, and B states, it is also loosely called E,F-B cascade. The E,F-B cascade also peaks in the low-energy region, around 18 eV, and becomes progressively smaller as electron energy increases. Both resonance and cascade preferentially populate the low *v_j* (=0–4) levels of the B state. The present measurement deals only with direct excitation.

For an excitation function measurement the grating was stationary, positioned at a strong emission feature, and isolated from other emissions with an appropriate slit width. Since the emissions from *v_j* = 0–4 of the B¹Σ_u⁺ state are known to be strongly enhanced by both resonance and E,F¹Σ_g⁺–B¹Σ_u⁺ cascade at low energies, the emission features and slit width were selected to minimize the interference of the emissions from these levels. H₂ gas pressure is also important, since high

pressure tenu-
cusses. Since
made for emi-
of the X¹Σ_g⁺
sion are there-
cm path leng-
sure.

The excite-
multiple sca-
started with
energy incre-
accumulated
energy was r-
nal was accu-
repeated un-
new scan wi-
was started.
added to the
previous sca-
the predeter-
accumulatio-
form during
had peak co-
scans. Dep-
the accumul-
The energy i-
eV (see belo-
ment were :
tral intensit-
μA. The su-
fects of shor-
pressure.

The mag-
the present
able cross-se-
trolled exp-
was found t-
measured sh-
found to be
electrons pr-
gun apertur-
by James ei-
shape functi-
the 13–250-
stability of
mental prot-
filament cha-
acquisition :
system coul-
data acquis-
sured with
~155 eV w-
the other fi-
ment. The
near the th-
imum at 5-
energy inc-
with the s-
number of

sented in
le effects.
ill be ad-

posure tends to introduce and enhance secondary processes. Since none of the measurements reported was made for emissions which terminate at the $v_i = 0$ level of the X $^1\Sigma_g^+$ state, the secondary absorption and emission are therefore negligible for measurements with ~ 11 cm path length and $10^{-4} \sim 5 \times 10^{-6}$ torr chamber pressure.

The excitation function measurement was a sum of multiple scans over the same energy range. Each scan started with the same initial electron beam energy and energy increment. After the photon emission signal was accumulated over a certain period of time, the electron energy was raised by a selected increment and the signal was accumulated and recorded. The process was repeated until the final energy was reached. Then, a new scan with the same initial energy and increment was started. The recorded photon emission signal was added to the signal at respective energy obtained in the previous scan. A measurement was completed when the predetermined number of scans was achieved. The accumulation time and energy increment were both uniform during the measurement. A typical measurement had peak counts of 2500–5000 and consisted of 10–25 scans. Depending on the photon emission intensities, the accumulation time was selected between 15 and 35 s. The energy increment was typically between 0.3 and 2.5 eV (see below). Electron currents used in the measurement were adjusted according to slit width and spectral intensities and were generally between 10 and 70 μA . The summation of multiple scans reduced the effects of short-term fluctuations of beam current and gas pressure.

The magnetically collimated electron gun used in the present experiment was found to show nonrepeatable cross-section shape functions. Under carefully controlled experimental conditions, the nonrepeatability was found to be 8%–13% (see next paragraph). The measured shape function at the high energy region was found to be dependent on lens voltages and secondary electrons produced by scattering off the H₂ gas and the gun apertures. These deviations, described in detail by James *et al.* [1997], limited the measurement of the shape function using the magnetically collimated gun to the 13–250 eV range in that experiment. The long-term stability of the gun filament also presented an experimental problem. The performance of the electron gun filament changed significantly in 20–40 days. The data acquisition time for some weak transitions of the H₂ Ly system could last as long as 4–7 days. To reduce the data acquisition time, excitation functions were measured with two separate sets of scans: one from 5 to ~ 155 eV with a 0.15–0.3 eV energy increment, and the other from ~ 5 to 1200 eV with a 2.3–2.5 V increment. The shape of the excitation function rises sharply near the threshold (11–15 eV) region, reaches a maximum at 50–60 eV, and then slowly decreases as the energy increases. The measurement from 5 to 155 eV with the smaller voltage step size yielded a sufficient number of data points to characterize the shape of the

low- to medium-energy regions, while the scan from 5 to 1200 eV permitted one to measure the shape from medium- to high-energy region without demanding too much acquisition time. The dual-scan method reduced the overall data acquisition time by a factor of 3–5 when compared to a single scan with uniform voltage increment.

Repeated measurement of an excitation (shape) function at the same experimental settings showed that the degradation of the filament over 3–6 days and variation of gas pressure and gun current during the measurement introduce 8%–13% errors. However, the primary source of error probably arises from the secondary electrons.

The P(1), P(2), and P(3) emissions of the (8,14) H₂ Ly band were selected to measure the B $^1\Sigma_u^+ - X ^1\Sigma_g^+$ excitation function. The P(1), P(2), and P(3) emissions occur at 1567.410, 1567.522, and 1567.248 Å, respectively. The spectral region 1566.9–1567.9 Å was selected for excitation function measurement. The contributions from resonance and cascade are negligible for emissions from the $v_j = 8$ level of the B $^1\Sigma_u^+$ state, and there are no other discrete emissions in the region [Liu *et al.* 1995]. The spectral region near the Q(1) line of the (1,4) H₂ W band at 1161.296 Å was selected for the W excitation function measurements. The R(0) emission of the (0,1) Ly band at 1161.694 Å, which is enhanced by resonance and cascade in the low-energy region, presented a problem for measurement near the Q(1) line of (1,4) band in the 1161.296 Å region. However, a 0.4 Å difference in wavelength position between Q(1) (1,4)W and R(0) (0,1)Ly makes it possible to minimize the interference of resonance and cascade effects from the R(0) (0,1) line by selecting appropriate slit position and width.

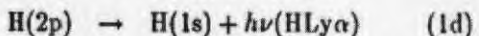
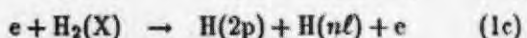
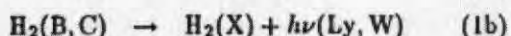
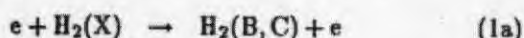
2.2. Determination of Relative B $^1\Sigma_u^+$ and C $^1\Pi_u$ State Excitation Functions From Emission Line Ratios

In many experimental and theoretical analyses the most important information is the relative shape (i.e., energy dependence) of the excitation function. The earlier work of SAH indicated significant differences between Ly and W shape functions. The differences in the current analysis with the earlier SAH work are primarily attributed to electron gun instability, secondary electron problems in the JPL experiment, and, to a lesser extent, difficulties in separating Ly and W emissions. In order to avoid experimental artifacts driven by temporal variation in electron gun parameters, we have compared cross sections by measuring relative line emission intensities obtained in high-resolution spectral scans at selected electron impact energies. The relative intensities of certain H₂ B - X and C - X emission lines in the 1200–1250 and 1335–1375 Å regions at 18, 20, 25, 50, 100, 250, and 500 eV excitation energies were obtained for this purpose. The measurements were performed by fixing the excitation energy at selected values and setting other gun parameters similar to those used in the

excitation function measurement. Relative intensities of emission lines in the two regions were recorded by scanning over the region with a 0.124 \AA (Full width at half maximum (FWHM)) resolution. This methodology was used to nullify the effects of electron gun instabilities.

2.3. H₂ and H Ly α Emission Cross Sections at 100 eV

We examine the following two reaction pairs:



Given an absolute cross section for (1a), the cross section for (1c) can be determined by experimentally measuring relative intensities of H Ly α and H₂ emission lines. This approach allows comparison of earlier accurate determinations of the cross section for (1c) and (1d) that were intended to be utilized as benchmark quantities.

Relative intensity measurements of H Ly α and H₂ emission were made between 1213 and 1225 Å with resolution (FWHM) of 0.10-0.11 Å and typical step size of ~ 0.020 Å. The relative sensitivity of the overall experimental system changes $\leq 2\%$ over the region [Liu et al., 1995]. Emissions from the (2,6) band of the W system provide prominent molecular features in the region. At 100 eV excitation energy the intensity of H Ly α emission is typically 17-50 times stronger than the intensities of the molecular hydrogen emission lines in the region. It is therefore important to ensure that the detecting system was not saturated by the strong H Ly α line. Relative intensities at 100 eV excitation energy were measured with various electron beam currents and H₂ chamber pressures over the range 5×10^{-6} - 1.5×10^{-4} torr. High-resolution (FWHM=0.10-0.11 Å) electron-impact-induced emission spectra near the H Ly α region make it possible to measure the intensity of H Ly α emission relative to certain molecular hydrogen transitions. Since the emission cross sections of H₂ emission lines are known, the atomic hydrogen H Ly α cross section can be obtained. Six spectral scans from 1213 to 1225 Å under different electron beam currents and chamber pressures were performed and analyzed. The beam current and gas pressure drifts during the scan were recorded and corrected. Data analysis involves correction of the background and measurement of the intensity of the H Ly α region relative to those of selected H₂ emission regions. The selected spectral regions of the H₂ emissions were 1218.7-1219.2 Å and 1223.3-1223.7 Å. The Q(1) and P(3) lines of the (2,6) H₂ W band are the primary molecular emissions for the first and second spectral regions, respectively. The selected wavelength region for H Ly α typically covers from 1215 to 1216.25 Å. Weak molecular lines underlying the H Ly α feature were taken into account in the analysis.

3. Theory

The volumetric photon emission rate I from electron-impact excitation is proportional to the excitation rate and emission branching ratio:

$$I_{ji} = g_j \frac{A_{ji}}{A_j} \quad (2)$$

where the indexes j and i refer to the upper and lower electronic state vibrational and rotational levels, respectively, and summation over the missing index is assumed. Here v and J refer to vibrational and rotational quantum numbers. $A(v_j, v_i; J_j, J_i)$ is the Einstein spontaneous transition probability for emission from level (v_j, J_j) to level (v_i, J_i) , and $A(v_j, J_j)$ is the total transition probability for level (v_j, J_j) . The excitation rate, $g(v_j, J_j)$, represents the sum of the excitation rate from the rotation and vibrational levels of the $X^1\Sigma^+$ state. The excitation rate is proportional to the population of the molecule at the initial level, $N(v_i, J_i)$, the excitation cross section σ and the electron flux F_e .

$$g_j = F_e \sum_i N_i \sigma_{ij} \quad (3)$$

The excitation cross section σ_{ij} can be obtained, in principle, by measuring the absolute photon-emission rate of a specific transition versus the excitation energy E . In practice, however, an accurate measurement of the absolute intensities is difficult. A relative intensity measurement is, instead, used to obtain the relative excitation function. The relative excitation function can be expressed in terms of an analytic collision strength Ω_{ij} [Shemansky *et al.*, 1985a, b].

$$\begin{aligned}\Omega_{ij} &= \frac{C_0}{X^2}(1 - 1/X) \\ &+ \sum_{k=1}^4 C_k(X-1) \exp(-kC_8 X) \\ &+ C_5 + \frac{C_6}{X} + C_7 \ln(X),\end{aligned}\quad (4a)$$

$$X = \frac{E}{E_{ii}}, \quad (4b)$$

$$\sigma_{ij} = \frac{\Omega_{ij}}{\omega E}, \quad (4c)$$

where E is the electron impact energy, E_{ij} is the transition energy, and ω_i is the degeneracy of the initial state. Energy in these equations is in Rydbergs, and cross sections are in units πa_0^2 . The coefficients C_k/C_l are determined by fitting the measured relative excitation function. If the transition is an electric dipole, the cross section can be placed on an absolute scale using the relationship

$$C_7 = \omega_i \frac{32\pi^2 m_e a_0^2}{h^2} \frac{f_{ij}}{E_{ij}}, \quad (5a)$$

$$C_7 = 4\omega_i \frac{f_{ij}}{E_{ii}} \quad (5b)$$

where m_e and m_h are respectively, the electron and hole mass; ϵ is the energy gap; E_{ij} is the transition strength. It is assumed that E_{ij} is constant over the absence of the transition. The transition strength is essentially constant for J_i or J_j (when given E) is next to zero. The electronic band structure of the vibrational quantum number Q was impeded by SAH. However, it has been shown that transitions exist between the transition J dependence of Liu et al.,¹ excitation energy.

4. Data A

The examination functions, as methods that provide absolute magnitude method, describe functions are due to excitation energy scans in magnitude of the the value of the optical absorption method (selective shapes through line intensities. The cross section of (1a), which is dent accurate experiments.

4.1. Energy Experiment

The first s
excitation en

where m_e and r_0 are electron mass and Bohr radius, respectively, and f_{ij} is the optical absorption oscillator strength. E_{ij} in (5b) is in Rydbergs.

It is assumed that C_k/C_7 ($k = 0 - 6$) and C_8 remain constant over all levels of a given electronic system. In the absence of perturbation and rotational dependence of the transition dipole matrix elements, the total collision strength of given upper state rotational levels is essentially constant. If the trivial variation of E_{ij} with J_i or J_j (which results in a slightly different X for a given E) is neglected, the total cross section of an electronic band system can be obtained by summing over vibrational quantum numbers only. The cross section of SAH was implicitly obtained using this approximation. However, it has been shown that a number of perturbations exist between the B $^1\Sigma_g^+$ and C $^1\Pi_u$ states, and the transition dipole matrix elements show a significant J dependence in some regions [Abgrall *et al.*, 1993a, b; Liu *et al.*, 1995]. Hence a statistically averaged total excitation cross section σ_s is more appropriate:

$$\sigma_s = \frac{1}{Q_p} \sum_{i,j} \sigma_{ij} N_i \quad (6)$$

where N_i is the rotational and vibrational population of the ground state target and Q_p is the partition function. At room temperature, all H₂ molecules populate the $v_i = 0$ level. The summation needs to be performed over J_i , v_i , and J_j only. When local perturbations and J dependence of the transition dipole matrix elements are absent, σ_s is identical to the conventional total cross section σ . If the dipole matrix element has a J dependence, the excitation cross section is temperature dependent (see section 5.2).

4. Data Analysis

The examination of the H₂ B-X and C-X excitation functions, as described in section 2, involves three methods that provide independent measures of the shape and absolute magnitudes of the cross sections. The first method, described in section 2.1, is one in which shape functions are established through analytic fits (4a)–(4c) to excitation functions obtained through electron energy scans in selected experiments. The absolute magnitude of the cross section is then established by fixing the value of the zero-order Born term using the known optical absorption oscillator strength (5a). The second method (section 2.2) independently determines the relative shapes of the B-X and C-X excitation functions through line intensity measurements at selected electron energies. The third method allows a determination of the cross section of (1c) from the derived cross sections of (1a), which can then be compared to several independent accurate measurements of (1c) and (1d) in earlier experiments. The analyses are described in turn below.

4.1. Energy-Scanned Electron Beam Impact Experiments

The first step in data analysis is calibration of the excitation energy. While energy step size can be mea-

sured accurately, the absolute energy scale is subject to experimental uncertainty. Two methods are used to establish the absolute energy scale of high-resolution (5–155 eV) scan. The first method involves measuring the appearance potential of the atomic hydrogen H Ly α emission. The difference between the absolute potential and measured appearance potential is then added to the recorded potentials of excitation function measurements. However, since the appearance potential of H Ly α depends on certain experimental conditions, such as lens voltages and pressure, the appearance potential needs to be measured each time when experimental conditions are changed. The second method, which is more convenient, refers to the known H₂ threshold energy of a specific transition. It involves a linear extrapolation and interpolation of the sharp rising cross-section curve near the threshold region back to the baseline. The energy at the intersection point is then compared with the known threshold energy. The difference is added to the measured data to obtain the calibrated energy. The energy scale obtained with these two methods agree with each other within 0.3–0.4 eV, which is comparable to or slightly smaller than the FWHM of the electron beam energy. Energy calibration with either the extrapolation/interpolation or H Ly α appearance potential method yields a large error (~ 2 eV) when used for measurement with a large energy increment. A third method, based on matching the shape of the excitation function in the region 12–150 eV, is also used. The accuracy of this calibration method is estimated to be 1 eV.

Once the energy scale is established, the background subtraction and data merge are performed. The averaged count value from the data points below the threshold energy is taken as background noise. After the background noise is subtracted from each data set, the high-resolution data set is merged with the low-resolution data set. The combination is typically performed with a 20–40 point average, which roughly corresponds to the energy region from 70 to 154 eV. The merged data set consists of the high-resolution data set from ~5 to 155 eV, and the scaled low-resolution data from 155 to 1200 eV.

Owing to the finite resolution of the spectrometer at the selected slit width, the measured excitation function generally involves a number of excitation-emission channels. The observed emission intensities are the sum of each excitation-emission channel weighted according to (2)–(5a). The weight factor for each excitation-emission channel is taken as the product of the population, C_7 , and the emission branching ratio. The measured intensities of the features near Q(1) of the (1,4) H₂ W band also have a small (less than 2% in the high-energy region) contribution from the H₂ Ly transitions. The H₂ Ly transitions are treated as if they had the same shape function as the W system. A nonlinear least squares program, based on the Marquard-Levenberg algorithm, is employed to determine the values of C_k/C_7 .

We find that the shape functions of H₂ Ly and W band systems, when measured under the same experi-

mental conditions, do not differ by more than 8%–13% between 18 and 100 eV. Differences typically occur in the 18 to 50 eV energy regions and become smaller at higher energy (essentially disappearing when the energy is above 250 eV). Below 18 eV the difference becomes larger than 13%, but the difference is attributed to resonance and cascade effects in the H₂ Ly system, rather than the direct excitation function of the B–X system.

The collision strength parameters C_k/C_7 are determined by combining the present measured data (13.5–250 eV) with the C–X cross section data obtained *De Heer and Carrière* [1971] because of electron gun instability in the present experiment at higher energy as discussed in section 2.1. The *De Heer and Carrière* [1971] C $^1\Pi_u$ cross section was obtained by measuring the shape function of the H₂ (3,7) W band and normalizing it to a theoretical Bethe cross section at 1500 eV. The *De Heer and Carrière* [1971] measurements were made with two experimental configurations, one for the low-energy region 50–500 eV, and the other for the high-energy region, 200–6000 eV [*Moustafa-Moussa et al.*, 1969]. Secondary electrons were suppressed in the high-energy configuration by establishing an interaction region with a lower potential than the collimator and Faraday cup [*Schram et al.*, 1965]. The accuracy of the electron energy was estimated to be 2 eV for the low-energy configuration and 20 eV for the high-energy configuration. The *De Heer and Carrière* [1971] C $^1\Pi_u$ state cross sections consist of 13 data points that range from 50 to 3000 eV. Since the threshold effect was not considered, the C $^1\Pi_u$ state cross section reported by *De Heer and Carrière* [1971], apart from a proportional constant, is also the shape function of the (3,0) band of the C–X excitation. The present data are combined with *De Heer and Carrière* [1971] data in the following way. First, the 13 data points reported by *De Heer and Carrière* [1971] are fitted to (4a). Since the data starts at 50 eV, the derived collision strength constants that are important in the low-energy region are not expected to be accurate. However, the C_5/C_7 ratio, which describes the shape function in the high-energy region is accurate and is obtained as $C_5/C_7 = -0.435$. Finally, parameters C_k/C_7 ($k=0-4$) and C_8 are determined from the present experimental data (13.5–250 eV) by constraining C_5/C_7 to -0.435. This approach not only effectively eliminates the instabilities of the JPL electron gun in the high-energy region but also minimizes the errors due to electron energy uncertainty (~20 eV in the high-energy configuration) in the measurements of *De Heer and Carrière* [1971].

Table 1 lists the collision parameters. Figure 1 shows the overplot of the experimental and model shape functions, based on excitation function measurement of P(1), P(2), and P(3) emission lines of the (8,14) Lyman band. The collision strength parameters C_k , for each excitation of the H₂ Ly and W band system can be computed by multiplying the relative value (C_k/C_7) in Table 1 with its C_7 . The H₂ Ly and W line transition probabilities calculated by *Abgrall et al.* [1987, 1993a, b, c] and *Abgrall and Roueff* [1989] and experimental energy levels obtained by *Dabrowski* [1984] and *Roncin*

and *Launay* [1994] are used to calculate C_7 . The total (direct) excitation cross section is calculated according to (6). Experimentally determined ground state energy levels reported by *Dabrowski* [1984] are also used to calculate the partition function.

Table 2 presents the total cross sections of the B $^1\Sigma_g^+$ and C $^1\Pi_u$ states at several excitation energies at room temperature (300 K). Figure 2 compares the B $^1\Sigma_g^+$ and C $^1\Pi_u$ state cross sections.

Cross sections in Table 2 are calculated by application of collision strength parameter ratios obtained from a nonlinear least squares fit of the present experimental data from 13.5 to 250 eV with the C_5/C_7 ratio fixed to -0.435 (Table 1). The ratio of C_5/C_7 is obtained from a nonlinear least squares analysis of the cross section shape function measured by *De Heer and Carrière* [1971]. While a moderate variation in the value of the C_5/C_7 ratio is expected to have some effect on the cross section, it is insignificant when compared with other experimental uncertainties. As the C_5/C_7 ratio changes, other collision parameters listed in Table 1 also vary correspondingly to fit the present experimental data, which covers the energy range from 13.5 to 250 eV. For example, when C_5/C_7 ratio is fixed at -0.596 (which is a 37% change from -0.435), the B–X and C–X cross sections at 100 eV decrease by only 9%. A ±50% change in the C_5/C_7 ratio results in less than a ±6% change in the cross section at 1200 eV. Since the present cross section is expected to have 12%–35% of error, the effect of statistical error in deriving C_5/C_7 ratio from *De Heer and Carrière* [1971] data is negligible. Analysis of the present data in the 13.5 to 1205 eV region (the entire present data range) with C_5/C_7 fixed to -0.435 is also performed. The cross section obtained from the analysis of the 13.5 to 1205 eV data (with C_5/C_7 again fixed to -0.435) does not differ significantly from that obtained from the corresponding analysis of 13.5 to 250 eV data. For example, the former is only 5%, 4%, 3%, 2%, and 0.5% smaller than the latter at 15, 50, 100, 300, and 500 eV, respectively.

4.2. Relative Line Intensity Measurements at Selected Electron Beam Energies

It is important to determine the relative shapes of the H₂ Ly and W systems for the purpose of obser-

Figure 1. measurement line. Nonl by solid li

Table 1. H₂ Lyman (Ly) and Werner (W) Collision Strength Parameters

Parameter ^a	Ratio
C_0/C_7	-0.01555195
C_1/C_7	-0.13491574
C_2/C_7	-0.02691103
C_3/C_7	0.32786896
C_4/C_7	-0.49744809
C_5/C_7	-0.435 ^b
C_6/C_7	0.435 ^b
C_8	0.17762538

^aSee equation (4a).

^bFixed by analysis of *De Heer and Carrière* [1971] data, see text.

$$S(Ly_j, I)$$

$$S(Wj, I)$$

where $S(j, E)$ is the emission line j , C_j , calibration factors also unknown in the energy E and for a given scan at the ratio

$$\frac{S(Ly_j, I)}{S(Wj, I)}$$

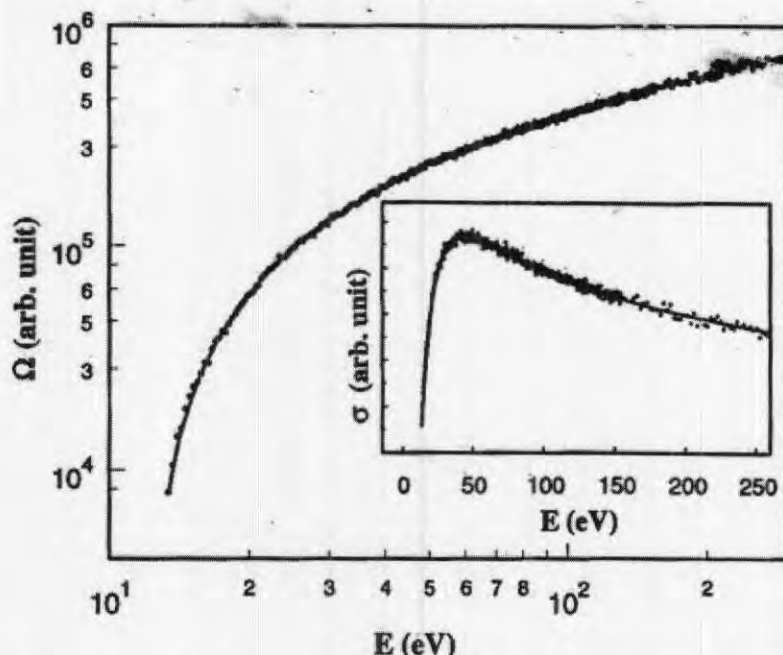


Figure 1. Collision strength and cross-section fits of H₂. Experimental data, which are based on measurement of the P(1), P(2), and P(3) lines of the (8,14) Lyman (Ly) band, are shown by dot line. Nonlinear least squares model data, obtained with C_5/C_7 constrained to -0.435, are shown by solid line. The inset compares the experimental and model cross-section shape functions.

vational diagnostics. Experimental results obtained by SAH suggest that the rising of the C-X shape function significantly lags the rising of the B-X shape function in the threshold region (see Figure 3). Electron energy loss measurements by Khakoo and Trajmar [1986], however, infer a larger C-X cross section relative to B-X at 20 eV. The current emission spectral measurements in the 1200-1350 Å region indicate that the C-X and B-X cross sections have similar shapes down to the threshold region. The method applied here is the only reliable approach to independently verify that electron gun instabilities have not seriously affected the determination of the shape functions. In this approach we measure individual emission line signals in the H₂ Ly and W systems at high resolution, under identical conditions at specific electron impact energies. The signal from given isolated emission lines can be described by

$$S(Lyj, E) = C_{Lyj} I(Lyj, E) \quad (7a)$$

$$= U_E U_{Lyj} \sigma(Lyj, E) \quad (7b)$$

$$S(Wj, E) = C_{Wj} I(Wj, E) \quad (7c)$$

$$= U_E U_W \sigma(Wj, E) \quad (7d)$$

where $S(j, E)$ is the measured signal from a particular emission line j , C_j , U_j are unknown experiment spectral calibration factors, and U_E defines excitation conditions also unknown in magnitude, but at a specific electron energy E and constant for a given spectral scan. For a given scan at energy E , U_E is eliminated by forming the ratio

$$\frac{S(Lyj, E)}{S(Wk, E)} = \frac{U_{Lyj}}{U_{Wk}} \frac{\sigma(Lyj, E)}{\sigma(Wk, E)} \quad (8)$$

The unknown constants U_j and U_k are eliminated by normalizing to a specific electron impact energy; in this case, 500 eV, where the zero-order Born term is dominant. Thus we form the ratio for specific lines,

$$\begin{aligned} & \left[\frac{S(Lyj, E)}{S(Wk, E)} \right] / \left[\frac{S(Lyj, 500)}{S(Wk, 500)} \right] \\ &= \left[\frac{\sigma(Lyj, E)}{\sigma(Wk, E)} \right] / \left[\frac{\sigma(Lyj, 500)}{\sigma(Wk, 500)} \right] \end{aligned} \quad (9)$$

Since excitation via the $P(J_i+1)$ and $R(J_i-1)$ transitions populates the same upper state level, each emission line involves more than one threshold energy. It is thus required that an assumed collision strength shape function be applied to the analysis, and if necessary, an iterative calculation is applied to establish the shape function. In this case we use the shape function established in section 4.1 and determine consistency with the measured emission spectra. We therefore scale each measured spectral line signal, $S(j, E)$, to form the normalized $S_0(j, E)$,

$$S_0(j, E) = \frac{S(j, E)}{P(j, E)} \quad (10a)$$

$$\sigma_0(j, E) = \frac{\sigma(j, E)}{P(j, E)} \quad (10b)$$

where $P(j, E)$ is the normalized shape function

$$P(j, E) = \sum_i \frac{N_i}{Q} \frac{1}{C_7} \frac{\Omega_{ji}(X)}{\omega_i E} \quad (11)$$

At $E = 500$ eV we normalize the cross-section ratio,

Table 2. Total H₂ Ly and W Cross Sections

E, eV	Lyman	Wener
12.0	3.51	0.00
12.2	6.40	0.00
12.4	10.3	0.68
12.6	15.1	2.07
12.8	20.6	4.81
13.0	26.5	8.73
13.3	36.3	15.9
13.6	46.4	24.2
14.0	59.8	36.1
14.5	76.0	51.2
15.0	91.3	65.7
15.5	106	79.3
16.0	119	92.0
16.5	131	104
17.0	143	115
17.5	154	126
18.0	164	135
18.5	174	145
19.0	183	153
20.0	199	169
22.5	232	201
25.0	255	224
27.5	273	242
30.0	285	254
35.0	301	270
40.0	308	278
45.0	310	281
50.0	308	281
60.0	301	276
70.0	291	267
80.0	281	258
90.0	271	250
100	262	241
150	225	208
200	198	184
250	177	165
300	160	149
350	146	136
400	134	125
450	124	116
500	115	108
600	101	94.9
700	90.7	85.0
800	82.3	77.1
900	75.4	70.7
1000	69.7	65.4
1100	64.9	60.9
1200	60.8	57.0
1300	57.2	53.7
1500	51.2	48.1
1700	46.5	43.7
2000	41.0	38.5
2500	34.3	32.3
3000	29.7	27.9

Units are 10^{-16} cm^2 , $T(\text{H}_2) = 300 \text{ K}$. E is excitation energy.

$$\frac{\sigma_0(\text{Lyj}, 500)}{\sigma_0(\text{Wk}, 500)} = 1.0, \quad (12)$$

and therefore have the relationship,

$$\left[\frac{S_0(\text{Lyj}, E)}{S_0(\text{Wk}, E)} \right] / \left[\frac{S_0(\text{Lyj}, 500)}{S_0(\text{Wk}, 500)} \right] = \frac{\sigma_0(\text{Lyj}, E)}{\sigma_0(\text{Wk}, E)} \quad (13)$$

If (13) calculated from the experiment deviates from a value of 1.0 beyond experimental error, a different shape function is inferred. Precautions were necessary in order to maintain accurate results: (1) The emission features whose intensity variations are compared were verified to be free of cascade enhancement. H₂ Ly emission lines originating from the $v_B \geq 5$ level between 1340 and 1375 Å were selected to compare against H₂ W Q branch emission lines in the 1200–1250 Å region. Contribution of E, F $^1\Sigma_g^+$ –B $^1\Sigma_u^+$ cascade excitation is insignificant at $v_B \geq 5$ levels. (2) The energy dependence of relative intensities must be considered in terms of threshold energy units. Threshold energy differences were accounted for by using a model program based on (2)–(4c) and applied to calculate $P(j, E)$ from 11.

Table 3 lists the spectral features used in this analysis, their approximate wavelength ranges, values of $S_0(j, E)$, and averaged values of (13) for all emission lines at five energies ranging from 18 to 100 eV. It should be stressed that the ratios are obtained by assuming that the shape functions of the two systems were identical (relation (11)). If the shape functions are, in fact, identical and errors due to relative intensity measurement and data analysis were negligible, ratios (13) would be unity. Thus the last row of Table 3, which lists the values obtained for (13), is a combination of experimental and data reduction errors as well as differences between the B and C state shape functions at 18, 20, 25, 50, and 100 eV. The difference at 250 eV (not shown in Table 3) is found to be $\sim 0.5\%$, a result consistent with the result from the energy scans that the H₂ Ly and W shape functions are essentially identical beyond 250 eV.

The total experimental and data analysis error (defined as the square root of the sum of squares of individual errors) in the relative intensity variation study is estimated to be 11%. Experimental errors due to the wavelength scale drift of the spectrometer, current and gas pressure changes during a scan as well as data analysis errors due to uncertainty in background subtraction can be estimated from the averaged standard deviation as a percentage of the averaged ratios in Table 3. The averaged standard deviation as a percentage of the ratio is 3.2%. The sum of data analysis errors and experimental error during the scans can be considered to be 3 times the average standard deviation as a percentage of the ratio, 9.5%. Since the analysis in Table 3 is made with the assumption that the electrons are strictly monoenergetic, errors due to the energy width of the electron beam also need to be considered. This error is estimated by comparing experimental data obtained at 20 eV with model outputs at 19, 20, and 21 eV. The comparison shows that the difference between Ly and W shape functions increases about 5% when the model excitation energy is lowered by 1 eV. Since the width (FWHM) of the electron beam in the present experiment is ~ 0.5 eV and absolute energy scale error is ~ 0.4 eV, the cross-section error due to the energy uncertainty of the electron beam can be taken to be 5% near 20 eV. The error due to the energy uncertainty is expected to increase significantly in the 12–17 eV region and become negligible above 50 eV. However, as long as

Figure
at 300
band:

the excitation &
intensity study

The H₂ Ly a
considered to b
of the present s
eV, the differen
listed in the las
or limit of the
stated in sectio

Table 3.

Wavelength Range (Å)
1206.5 –
1218.8 –
1223.3 –
1229.7 –
1239.3 –
1247.2 –
1341.6-1
1343.4-1
1350.3-1
1350.7-1
1361.8-1
1363.8-1
1365.4-1
1367.7-1
1369.9-1
1370.2-1

$[\sigma_0(\text{Lyj}, E)]$

^aSee eq

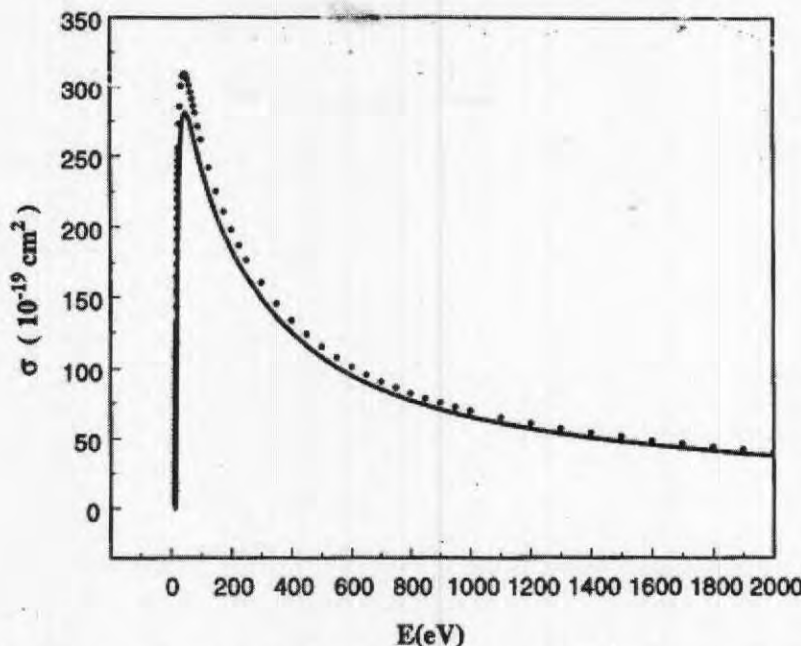


Figure 2. Total cross sections (in 10^{-19} cm^2) of the Lyman (Ly) and Werner (W) band systems at 300 K. The cross section of the Ly band system is represented by dots, while that of the W band system is shown by the solid line.

the excitation energy is greater than 18 eV, the relative intensity study has 11% overall error.

The H₂ Ly and W excitation shape functions can be considered to be identical within the experimental error of the present study. Except for the measurement at 25 eV, the differences between Ly and W shape functions listed in the last row of Table 3 are within the 11% error limit of the relative intensity variation study. As stated in section 2, the nonrepeatability of the present

shape function measurements is 8%-3%. The cross sections are therefore considered to have the same energy dependence on a threshold energy scale.

4.3. DISSOCIATIVE EXCITATION CROSS SECTION OF H₂ LY α EMISSION

The measurements described in section 2.3 reduce to a cross section for the reaction (1c) of

Table 3. H₂ Ly and W Excitation Functions From Line Emission Strengths

Wavelength Range (Å)	Transitions J(v _j , v _i)Br	$S_0(j, E)$					
		18 eV	20 eV	25 eV	50 eV	100 eV	500 eV
1206.5 - 1206.8	1(1,5)Q	2250	1785	6600	3050	4250	3300
1218.8 - 1219.1	1(2,6)Q	2300	1820	6600	3050	4350	3400
1223.3 - 1223.6	3(2,6)P	2100	1690	6300	3050	4300	3300
1229.7 - 1230.1	1(3,7)Q	2150	1685	6250	3050	4400	3150
1239.3 - 1239.7	1(4,8)Q	2150	1625	6000	2900	4250	3100
1247.2 - 1247.5	1(5,9)Q	2125	1600	6000	2675	4150	3075
<i>Werner</i>							
1341.6-1341.9	3(5,6)P/2(12,9)P	1675	...	6000	2900	4000	2950
1343.4-1343.7	1(7,7)R	2025	1695	6300	3000	3950	2950
1350.3-1150.7	3(7,7)R/0(9,8)R	6300	2900	3850	2800
1350.7-1351.1	1(9,8)R	2025	1695	6600	2900	4000	2950
1361.8-1262.1	3(11,9)P/3(15,11)P	1875	...	6100	2800	3800	2850
1363.8-1364.1	1(6,7)R	2000	1725	6700	...	3850	2950
1365.4-1365.8	1(6,7)P	1775	1525	6200	2850	3850	2800
1367.7-1368.1	2(6,7)P	1800	1575	6000	2700	3700	2700
1369.9-1370.3	0(8,8)R	6650	...	3800	2850
1370.2-1370.5	1(8,8)R	2000	1625	6450	2700	3850	2800
$[\sigma_0(Lyj, E)/\sigma_0(Wj, E)]^a$		0.978	1.087	1.133	1.093	1.016	

^aSee equation (13).

Table 4. Temperature Dependence of H₂ Lyman Cross Sections

E, eV	Temperature, K							
	10	30	50	100	300	500	1000	3000
12.4	9.934	9.941	9.988	10.09	10.31	10.59	11.44	21.98
12.6	14.68	14.69	14.74	14.85	15.11	15.44	16.42	27.86
12.8	20.13	20.14	20.20	20.32	20.61	20.98	22.08	34.29
13.0	26.06	26.07	26.13	26.26	26.58	27.03	28.29	41.13
13.3	35.36	35.39	35.53	35.82	36.28	36.82	38.23	51.82
13.6	44.97	45.01	45.27	45.80	46.40	46.99	48.49	62.67
14.0	57.77	57.83	58.24	59.07	59.83	60.47	62.06	76.95
14.5	73.25	73.34	73.92	75.06	76.02	76.73	78.42	94.01
15.0	87.91	88.02	88.74	90.18	91.31	92.07	93.83	110.0
16.0	114.4	114.6	115.6	117.5	119.0	119.8	121.7	138.9
17.0	137.6	137.8	139.0	141.5	143.1	144.1	146.0	164.1
18.5	167.0	167.3	168.8	171.8	173.9	174.9	177.0	196.0
20.0	191.2	191.5	193.3	196.8	199.1	200.2	202.4	222.1
22.5	222.4	222.8	224.9	229.0	231.7	232.8	235.1	255.6
25.0	245.2	245.5	247.9	252.5	255.4	256.6	259.0	279.9
27.5	261.8	262.2	264.7	269.7	272.8	274.0	276.4	297.4
30.0	273.9	274.3	276.9	282.2	285.4	286.6	289.0	310.0
35.0	288.6	289.0	291.8	297.4	300.8	302.0	304.4	325.1
40.0	295.2	295.7	298.6	304.3	307.7	309.0	311.3	331.5
50.0	295.8	296.2	299.2	304.9	308.3	309.6	311.7	330.8
70.0	279.3	279.7	282.5	288.0	291.2	292.3	294.2	311.1
100	251.1	251.5	254.0	258.9	261.8	262.8	264.4	279.1
150	216.0	216.3	218.5	222.7	225.2	226.0	227.4	239.6
200	190.3	190.6	192.5	196.3	198.4	199.2	200.4	210.8
500	110.4	110.5	111.6	113.8	115.1	115.5	116.1	121.6
750	82.72	82.84	83.68	85.32	86.26	86.56	87.03	91.08
1000	66.87	66.97	67.65	68.98	69.74	69.98	70.35	73.60
1500	49.13	49.20	49.70	50.68	51.23	51.41	51.68	54.04
2000	39.27	39.33	39.73	40.51	40.95	41.09	41.31	43.18
3000	28.46	28.50	28.79	29.35	29.68	29.78	29.93	31.28

Units are 10^{-19} cm^2 .

Table 5. Te

E, eV

12.4

12.6

12.8

13.0

13.3

13.6

14.0

14.5

15.0

16.0

17.0

18.5

20.0

22.5

25.0

27.5

30.0

35.0

40.0

50.0

70.0

100

150

200

500

750

1000

1500

2000

3000

Units are 10

$$\sigma(H\text{Ly}\alpha, 100\text{eV}) = (7.16 \pm 0.95) \times 10^{-18} \text{ cm}^2 \quad (14)$$

determined relative to the H₂ W absolute cross section obtained here. The error limit is 3 times the standard deviation obtained by analysis of six sets of emission spectra. The uncertainties in background correction, particularly for the scans obtained at low pressure (5×10^{-6} torr), and slight wavelength shift resulting from nonuniform step size are the two most important sources of error. Uncertainty in the H₂ C $^1\Pi_u$ state cross section at 100 eV has not been included in the error estimate.

5. Discussion

Table 1 lists the collision parameters (4a) derived from the analytic fitting process described in section 4.1. Figure 1 shows the superposition of the experimental and model shape functions, based on measurement of P(1), P(2), and P(3) emission lines of the (8,14) H₂ Ly band.

5.1. Total Excitation Cross Section

The collision strength parameters C_k for each fine structure excitation of the H₂ Ly and W band systems can be computed by multiplying the relative value

($C_k/C_7, k = 0 - 6$) in Table 1 with the appropriate value of C_7 . H₂ Ly and W line transition probabilities calculated by Abgrall et al. [1987, 1993a, b, c] and Agrall and Roueff [1989] and experimental energy levels obtained by Dabrowski [1984] and Roncin and Launay [1994] are used to calculate C_7 through (5a). The total direct (1a) excitation cross section is calculated according to (6). Experimentally determined ground state energy levels reported by Dabrowski [1984] are used to calculate the partition function.

The total cross sections of the B $^1\Sigma_u^+$ and C $^1\Pi_u$ states are given in Table 2 at several excitation energies at room temperature (300 K). Figure 2 compares the B $^1\Sigma_u^+$ and C $^1\Pi_u$ state cross sections. Cross sections in Table 2 are calculated by assuming that all excitation transitions have the same shape as given in Table 1. While a moderate variation in the shape function is expected, this factor is insignificant relative to other experimental uncertainties.

5.2. Temperature Dependence

Temperature dependence of the H₂ Ly and W cross section is caused by J dependence of the transition dipole matrix elements and local perturbations between the B $^1\Sigma_u^+$ and C $^1\Pi_u^+$ states. J dependence of the transition dipole matrix elements primarily arise from the

centrifugal d prevents a c from vibratio small mass of matrix eleme is large for ce Liu et al., 198 C $^1\Pi_u^+$ states strength. Per zero-order osc $^1\Pi_u^+$ states. the cross sect 2-5% lower, been 2-5% la J dependence and local per cillator streng change in the tions and the Tables 4 a Ly and W be 3000 K at sev of the B $^1\Sigma_u^+$ However, exc

Table 5. Temperature Dependence of H₂ Werner Cross Sections

E, eV	Temperature, K								
	10	30	50	100	300	500	1000	3000	
3000									
21.98	12.4	0.597	0.598	0.608	0.629	0.677	0.740	0.950	4.64
27.86	12.6	1.866	1.87	1.89	1.95	2.07	2.23	2.67	7.49
34.29	12.8	4.56	4.57	4.60	4.66	4.81	5.01	5.60	11.32
41.13	13.0	8.35	8.36	8.41	8.52	8.73	8.96	9.65	16.04
51.82	13.3	15.69	15.69	15.68	15.66	15.86	16.13	17.04	24.27
62.67	13.6	24.38	24.37	24.26	24.05	24.20	24.53	25.61	33.40
76.95	14.0	36.82	36.79	36.55	36.08	36.15	36.53	37.76	46.03
94.03	14.5	52.48	52.42	52.03	51.27	51.22	51.62	52.99	61.59
110.0	15.0	67.49	67.41	66.88	65.86	65.69	66.10	67.56	76.32
138.9	16.0	94.78	94.67	93.88	92.37	91.98	92.42	94.02	103.1
164.1	17.0	118.8	118.6	117.6	115.7	115.1	115.5	117.3	126.4
196.0	18.5	149.4	149.2	147.9	145.4	144.6	145.1	146.9	156.3
222.1	20.0	174.8	174.5	173.0	170.0	169.0	169.5	171.5	180.9
255.6	22.5	207.8	207.5	205.7	202.1	200.8	201.2	203.4	212.8
279.9	25.0	232.1	231.8	229.7	225.7	224.2	224.7	226.9	236.2
297.4	27.5	250.1	249.7	247.5	243.2	241.5	242.0	244.2	253.4
310.0	30.0	263.4	263.0	260.7	256.1	254.3	254.7	257.1	266.0
325.1	35.0	280.2	279.8	277.3	272.4	270.4	270.9	273.2	281.7
331.5	40.0	288.4	288.0	285.4	280.4	278.3	278.8	281.1	289.1
330.8	50.0	291.3	290.9	288.3	283.1	281.1	281.4	283.7	290.9
311.1	70.0	277.3	276.9	274.4	269.4	267.4	267.7	269.7	275.8
279.1	100	250.2	249.9	247.6	243.2	241.3	241.6	243.3	248.5
239.6	150	215.9	215.6	213.6	209.8	208.2	208.4	209.9	214.1
210.8	200	190.8	190.6	188.8	185.4	184.0	184.2	185.5	189.0
121.6	500	111.7	111.6	110.5	108.5	107.7	107.8	108.5	110.1
91.08	750	83.88	83.76	82.99	81.49	80.85	80.92	81.43	82.63
73.60	1000	67.87	67.77	67.15	65.93	65.41	65.47	65.88	66.83
54.04	1500	49.91	49.84	49.38	48.49	48.10	48.14	48.44	49.12
43.18	2000	39.92	39.86	39.50	38.78	38.47	38.50	38.74	39.28
31.28	3000	28.95	28.91	28.64	28.12	27.90	27.92	28.10	28.48

Units are 10⁻¹⁹ cm².

iate val
lities cal
and Al
and A
d Laun
The tota
d accord
state en
e used to

d C ¹Π_u
energies
pares the
sections
ll excita
in Table
function to other

W cross
transition
between the
the trans
from the

centrifugal distortion potential, $J(J+1)/2\mu R^2$, which prevents a complete separation of rotational motion from vibrational and electronic motions. Because of the small mass of H₂, J dependence of the transition dipole matrix elements (and therefore the oscillator strength) is large for certain transitions [Abgrall et al., 1993a, b; Liu et al., 1995]. Perturbations between the B ¹Σ_u⁺ and C ¹Π_u⁺ states introduce irregular variations of oscillator strength. Perturbations also cause the partitioning of zero-order oscillator strength between the B ¹Σ_u⁺ and C ¹Π_u⁺ states. Had the local perturbations been absent, the cross section of the B ¹Σ_u⁺ state would have been 2–5% lower, and that of the C ¹Π_u⁺ state would have been 2–5% larger than those listed in Table 2. Both the J dependence of the transition dipole matrix elements and local perturbations result in an irregularity in oscillator strength. Variation of temperature causes the change in the population weight of the irregular transitions and therefore the total cross sections.

Tables 4 and 5 give the total cross sections of H₂ Ly and W band systems, respectively, between 10 and 3000 K at several excitation energies. The cross section of the B ¹Σ_u⁺ state increases with rising temperature. However, except at very low energy, the cross sections

of the C ¹Π_u⁺ state first decrease and then increase as temperature rises.

Perturbations between the B ¹Σ_u⁺ and C ¹Π_u⁺ states are responsible for the anomalous temperature dependence of the C ¹Π_u⁺ state cross section. As mentioned earlier, the coupling between the states results in mixing of zero-order wave functions and therefore partitioning of the oscillator strength. The total oscillator strengths of the H₂ Ly and W bands are 0.311 and 0.356, respectively, according to the calculation of Allison and Dalgarno [1970] [see also Chan et al., (1992) Table 3]. The B ¹Σ_u⁺ state has 38 vibrational levels while the C ¹Π_u⁺ state has only 14 vibrational levels. Since about half of the H₂ W band oscillator strength goes into the X ¹Σ_g⁺ – C ¹Π_u⁺ (P and R branch) excitation, it follows that the rotational line oscillator strength of the C ¹Π_u⁺ (or C ¹Π_u) state, on average, is larger than that of the B ¹Σ_u⁺ state. Therefore perturbations generally result in transfer of (zero order) oscillator strength from the perturbed levels of the ¹Π_u⁺ state into their counterparts of the B ¹Σ_u⁺ state. Most of the perturbations take place in $J > 1$ levels, so the C ¹Π_u⁺ cross section first decreases with rising temperature. When the B ¹Σ_u⁺ and C ¹Π_u⁺ state cross sections are considered together, the effects

of perturbations approximately cancel out. The (B+C) cross section always increases with increasing temperature.

Near threshold the cross sections rise extremely rapidly with increasing energy. The temperature effect is particularly significant because higher temperature puts more weight in higher rotational (and vibrational) levels. Tables 4 and 5 also show that a drastic increase in the B $^1\Sigma_u^+$ and C $^1\Pi_u$ state cross sections in the threshold region as the temperature rises from 1000 to 3000 K. Such a sharp increase is primarily due to the excitation of the rotational manifold of the $v_i = 1$ level. While less than 0.3% of H₂ is in the $v_i = 1$ manifold at 1000 K, more than 12.3% of population at 3000 K is in the $v_i = 1$ manifold.

Cross sections in Tables 4 and 5 are obtained using (6). Equation (6) can also be applied to nonthermal equilibrium conditions, given known values of N_i .

5.3. Comparison With SAH

While this work follows the same principle and approach outlined by SAH, several important differences exist between the present and previous work. Experimentally, the present work utilizes a high-resolution spectrometer and measures the excitation function at resolutions of (FWHM) 0.35–2.5 Å, while the previous work obtained the excitation function at resolutions of (FWHM) 5–10 Å resolution. As a result, the number of excitation channels that contribute to the measured excitation function is reduced from 40–50 to 5–10, and complications arising from resonance and cascade are greatly decreased. While SAH utilized the Allison and Dalgarno [1970] oscillator strengths and scaled them down by 8% and 15%, respectively, the present study uses the more accurate rotational line oscillator strength of Abgrall *et al.* [1987, 1993 a, b, c] and Abgrall and Roueff [1989]. Furthermore, the theoretical calculations of Dressler and Wolniewicz [1985] show that the downscaling is not correct. SAH also treated all the rotational excitations of a vibrational band as if they had identical threshold energies and neglected the variations of transition dipole matrix elements with rotational quantum number and perturbations between the B $^1\Sigma_u^+$ and C $^1\Pi_u^+$ states. Differences in threshold energy of each rotational excitation and J dependence of the transition dipole matrix elements as well as perturbations are fully considered in the present work. Consideration of the differences in excitation threshold energy is very important near the threshold region, where a small change in excitation energy will open or close many excitation channels (see Tables 4 and 5). As a result of these differences, the present cross sections differ from SAH cross sections even in the medium-energy region. For example, the B $^1\Sigma_u^+$ and C $^1\Pi_u$ state cross sections given by SAH are 2.67×10^{-17} and 2.78×10^{-17} cm², respectively, at 100 eV and 1.85×10^{-17} and 1.93×10^{-17} cm², respectively, at 200 eV. The corresponding cross sections obtained in the present work are 2.62×10^{-17} and 2.41×10^{-17} cm² at 100 eV and 1.98×10^{-17} cm² and 1.84×10^{-17} cm² at 200 eV. In addition,

the SAH B/C cross section ratio at 20 eV is 5.4, while the present ratio is ~1.2, which is fairly close to the 1.4 obtained by Khakoo and Trajmar [1986]. The discrepancies between the excitation cross sections of SAH and those of the present are also partially due to the differences in the shape functions. For example, the B $^1\Sigma_u^+$ and C $^1\Pi_u$ shape functions obtained in this work are very similar and are considered to be identical, while the B $^1\Sigma_u^+$ and C $^1\Pi_u^+$ shape functions measured in the previous work differ significantly, particularly in the low-energy regions.

Figure 3 compares the present and previous excitation cross sections. To make a relevant comparison, both previous and present cross sections are calculated with the rotational line transition probabilities of Abgrall and Roueff [1989] and Abgrall *et al.* [1993a, b, c]. Several differences can be seen in Figure 3. First, the inserted plot shows that B $^1\Sigma_u^+$ and C $^1\Pi_u$ state excitation functions of SAH overestimate the peak cross sections by 20–30%. In addition, the energy corresponding to the peak cross section of the C $^1\Pi_u$ state in the previous work (~70 eV) is higher than the value in this work (~45 eV) by about 25 eV, although the peak energies of the B $^1\Sigma_u^+$ state in both works (~45 eV) are in agreement. As Figure 3 shows, the SAH collision strength curve of the C $^1\Pi_u$ state does not reach the level of other three curves until 30–35 eV. More extreme differences occur in threshold region. While the earlier B $^1\Sigma_u^+$ state cross section rises slightly more slowly than its new B $^1\Sigma_u^+$ state counterpart, the earlier C $^1\Pi_u$ state cross section rises much more slowly than the present C $^1\Pi_u$ state cross section. Between 12.5 and 17.5 eV energy regions, the earlier B $^1\Sigma_u^+$ shape function falls below the present cross section by a factor of 4.3 to 1.2, while the earlier C $^1\Pi_u$ function falls below the present values by factors of 496 to 8.1. It is the slow rising of the earlier C $^1\Pi_u$ function that results in an abnormally large B/C state cross section ratio in the threshold and low-energy region.

5.4. Comparison With Other Experiments

Table 6 lists our total excitation cross sections of the Lyman and Werner band systems at several excitation energies, together with the experimental cross sections of Khakoo and Trajmar [1986], and Srivastava and Jensen [1977]. Khakoo and Trajmar estimated experimental error of the cross sections to be 19%–21%.

Table 6 shows that our H₂ Ly cross sections are in good agreement with those obtained by Khakoo and Trajmar [1986]. The largest difference occurs at 30 eV, where our cross section is ~17% larger than that of Khakoo and Trajmar [1986]. On the other hand, the differences between our cross section and that of Srivastava and Jensen [1977] are much larger. This work obtained 308.3×10^{-19} cm² for 50 eV, whereas Srivastava and Jensen [1977], after renormalization and interpolation by Trajmar *et al.* [1983], yielded 240×10^{-19} cm². While the renormalized Srivastava and Jensen [1977] cross section is ~28% smaller, it is still close to our experimental error limit, ~25% near 50 eV. How-

Fig.
[198
whil
line

ever, the ren
Jensen [1977
most 2 times
The differenc
(30%–35%)

The Srivastava
obtained by
measure the
level of the 1
60 eV and s
inal data we

Table 6. C
tions

E, eV	P _i
15	17
20	1
30	1
40	1
50	1
60	1

Units are 11
*Source is
indicated.

^bSource is
recommended.

^cValue req.

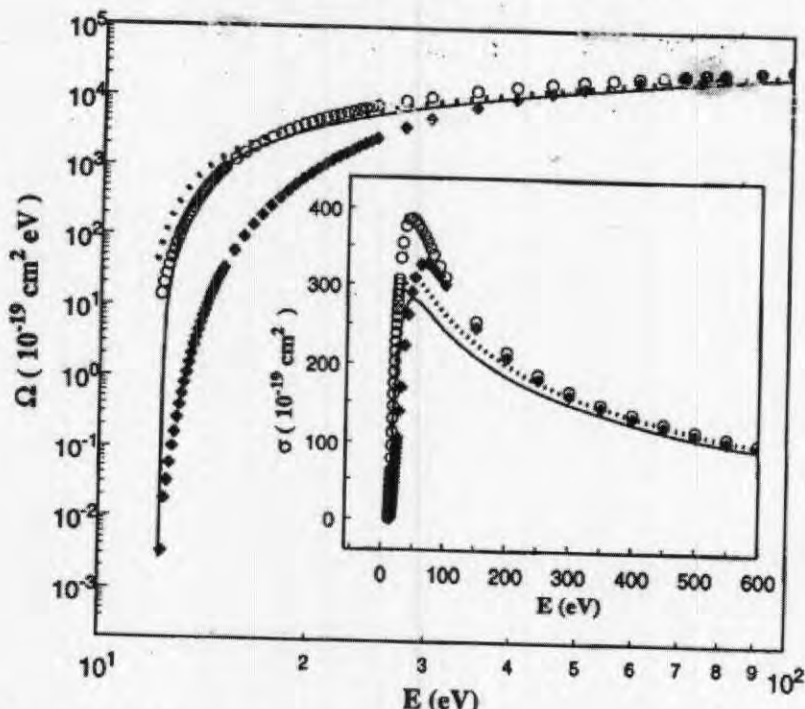


Figure 3. Comparison of the collision strengths and cross sections (inset) of Shemansky et. al. [1985a] with those of this study. The Shemansky et. al. data for Ly are shown by open circles while W data are denoted by solid diamonds; this study data for Ly are represented by dotted line while data for W are denoted by the solid line.

eV is 5.4 eV is 5.4
ly close to 986]. The sections of
illy due to
example,
ed in this
identical,
measured
icularly in

us excita-
mparison,
calculated
ies of Ab-
93a, b, c].
First, the
state ex-
peak cross
rrespond-
ate in the
ue in this
peak en-
5 eV) are
collision
reach the
extreme
he earlier
only than
¹Π_u state
e present
17.5 eV
tion falls
.3 to 1.2,
e present
rising of
normally
hold and

ever, the renormalized cross section of Srivastava and Jensen [1977] at 15 eV is $(170 \pm 50) \times 10^{-19} \text{ cm}^2$, almost 2 times larger than our result, $91.3 \times 10^{-19} \text{ cm}^2$. The difference far exceeds our experimental uncertainty (30%–35%) at 15 eV.

The Srivastava and Jensen [1977] cross sections were obtained by using electron energy loss techniques to measure the differential cross sections of the $v_f = 2$ level of the $B^1\Sigma_u^+$ state for excitation energies of 15–60 eV and scattering angles of 10° to 135°. The original data were normalized with H₂ elastic differential

cross sections, which, in turn, were normalized by He differential cross sections. The Srivastava and Jensen [1977] cross sections were subsequently renormalized by Trajmar et al. [1983]. The renormalized cross sections at 15 and 50 eV are listed in Table 6.

There are several possible explanations for the large difference between our excitation cross section and that of Srivastava and Jensen [1977] at 15 eV. First, Srivastava and Jensen [1977] neglected the difference in threshold energies for excitations to various vibration and rotation levels of the $B^1\Sigma_u^+$ state. Since the cross section changes sharply with excitation energy in the threshold regions, the neglect of the difference in threshold energy seriously overestimates the contribution of excitations to higher ($v > 2$) vibrational levels of the $B^1\Sigma_u^+$ state. While the difference in threshold energy was also not considered in the work of Khakoo and Trajmar [1986], its effect on cross section is significantly less important at 20 eV or higher energy than 20 eV. In addition, the renormalized Srivastava and Jensen [1977] cross sections are significantly larger than the cross sections of Khakoo and Trajmar [1986] as well as the values of this study. For example, the Srivastava and Jensen [1977] $B^1\Sigma_u^+$ state cross section at 20 eV is $(250 \pm 70) \times 10^{-19} \text{ cm}^2$, which is ~26% and ~18% larger than the $199 \times 10^{-19} \text{ cm}^2$ obtained in this work and $212 \times 10^{-19} \text{ cm}^2$ obtained by Khakoo and Trajmar [1986]. Finally, the error in the absolute energy between two studies can be different. A ±0.5 eV error in energy scale at 15 eV for a monoenergetic electron beam introduces about ±17% of error in the H₂ Ly cross section. The cross-

Table 6. Comparison of Experimental H₂ Cross Sections

E, eV	Lyman		Werner	
	Previous*	Present	Previous*	Present
15	170 ± 50^b	91.3	...	65.7
20	212.4	199.1	155.8	169.0
30	243.7	285.4	176.0	254.3
40	303.7	307.7	196.1	278.3
50	$240^{b,c}$	308.3	...	281.1
60	295.1	301.1	222.0	275.7

Units are 10^{-19} cm^2 .

*Source is Khakoo and Trajmar [1986], unless otherwise indicated.

^bSource is Srivastava and Jensen [1977], renormalized as recommended by Trajmar et al. [1983].

^cValue requires an interpolation.

section difference suggests that the absolute energy of Srivastava and Jensen [1977] is too high and/or the energy scale of the present study is too low. It should be noted that any one of the above explanations is insufficient to account for the large difference of cross sections at 15 eV. A plausible explanation requires all the factors to act in concert.

Table 6 also includes a comparison of the present cross sections of the H₂ W band system with those reported by Khakoo and Trajmar [1986]. In general, the differences between the C $^1\Pi_u$ state cross sections are larger than the differences between the B $^1\Sigma_g^+$ state cross sections. Our C $^1\Pi_u$ state cross sections are larger at all energies than those of Khakoo and Trajmar [1986]. While differences at 20 eV (8%) and 60 eV (24%) are within our experimental error, discrepancies at 30 eV (44%) and 40 eV (42%) are significantly larger than our experimental errors. The B/C cross section ratios obtained by Khakoo and Trajmar [1986] are 1.36, 1.38, 1.55, and 1.33 at 20, 30, 40, and 60 eV, respectively. The ratios at the same energies in this study, which uses an identical shape function for B $^1\Sigma_g^+$ and C $^1\Pi_u$ states, are 1.18, 1.12, 1.11, and 1.09. If the B $^1\Sigma_g^+$ and C $^1\Pi_u$ shape functions are similar or identical (in terms of threshold energy units, X), the B/C cross-section ratio should decline monotonically with increasing excitation energy and approach a limit of slightly less than 1.0, since the threshold effect favors the C $^1\Pi_u$ state at high energy and the integrated total oscillator strength of the C $^1\Pi_u$ - X $^1\Sigma_g^+$ transition is slightly larger than that of the B $^1\Sigma_g^+$ - X $^1\Sigma_g^+$ transition. The work of Khakoo and Trajmar [1986] suggests that the C $^1\Pi_u$ state shape function differs significantly from the B $^1\Sigma_g^+$ state and that, when normalized to a common C_7 value, the C $^1\Pi_u$ shape function is 15%, 23%, 40%, and 22% smaller than the B $^1\Sigma_g^+$ shape function at 20, 30, 40, and 60 eV, respectively. However, our relative intensity analysis, as a function of excitation energy (Table 3), indicates the C state shape function, when normalized to the same value of C_7 , is smaller than B state shape function by (at most) 13.3% between 20 eV and 50 eV. Thus the present study suggests that the experimental error in the Khakoo and Trajmar [1986] work could be significantly larger than 21%. Indeed, the error analysis of Khakoo and Trajmar [1986] was not rigorous, and the error in some cases could be as large as 35–40% (S. Trajmar, private communication, 1996; M. A. Khakoo, private communication, 1997).

Table 7 compares the present C $^1\Pi_u$ state cross section with that determined by De Heer and Carrière [1971]. The C $^1\Pi_u$ state cross section reported by De Heer and Carrière [1971] was obtained by normalizing the (3, 7) band excitation function to the theoretical Bethe cross section of the C $^1\Pi_u$ state at 1500 eV. As Table 7 shows, the C $^1\Pi_u$ state cross section reported by De Heer and Carrière [1971] are 33%–16% larger than the present cross section, with the largest differences in the low-energy region. Table 7 also shows the C $^1\Pi_u$ state cross section of De Heer and Carrière [1971] rescaled to the present C $^1\Pi_u$ state cross section at 1500

Table 7. Comparison of De Heer and Carrière [1971] and Present H₂ W Cross Sections

E, eV	De Heer and Carrière [1971] ^a		Present Study
	Original ^a	Rescaled ^b	
50	359.	300.	281.
100	320.	268.	241.
150	268.	224.	208.
200	231.	193.	184.
300	187.	156.	149.
400	152.	127.	125.
500	133.	111.	108.
600	114.	95.4	94.9
800	95.1	79.5	77.1
1000	81.0	67.8	65.4
1500	57.5	48.1	48.1
2000	44.5	37.2	38.5
3000	32.4	27.1	27.9

Units are 10^{-19} cm^2 .

^aData are from De Heer and Carrière [1971, Table 1].

^bValues are normalized to present cross section at 1500 eV.

eV. As expected, the differences between the rescaled and present cross sections are very small (<5%) when excitation energy is ≥ 200 eV. The largest differences, again, occur in the low-energy region and are 6.8% and 11% at 50 and 100 eV, respectively. The large differences in the low-energy region are due to more accurate measurements and more data points in the present experiment, as well as the neglect of the differences in threshold energies of various excitations by De Heer and Carrière [1971]. However, all the differences are less than our experimental error, estimated to be 7%–25% at 50 to 3000 eV.

5.5. Comparison to Theory

Most theoretical calculations of dipole-allowed excitation cross sections are limited to the B-X transitions [Chung and Lin, 1978; Fliflet and McKoy, 1980; Gibson et al., 1987], although calculation of B' $^1\Sigma_g^+$ and C $^1\Pi_u$ are also available [Arrighini et al., 1980; Redmon et al., 1985]. Table 8 compares the cross section of the B $^1\Sigma_g^+$ state determined by this study with those calculated by various techniques. The Born cross sections in Table 8 are obtained by the present authors from numerical integration of the general oscillator strengths calculated by Kolos et al. [1982a, b, 1983] and Szalewicz et al. [1984]. The numerical integration error is <5%, as indicated by the good agreement with the Born cross section obtained by Fliflet and McKoy [1980].

There are significant differences (Table 8) between the experimental and calculated cross sections, with theoretically calculated cross sections always larger than the present cross sections. Table 8 is consistent with the observation by Celiberto and Rescigno [1993] that the calculated H₂ Ly system cross section is ~ 2 times larger than the experimental cross section in the range of 20–60 eV. The largest differences typically occur at

Table 8. Comparison of De Heer and Carrière [1971] and Present H₂ W Cross Sections

E, eV	P ^a
50	91.3
70	199
100	255
150	285
200	301
300	308
400	310
500	308
600	301
700	291
1000	281
1500	221
2000	191
3000	161
4000	131
5000	111
6000	101
7000	901
8000	821
9000	751
10000	691
11000	641
12000	601
13000	571

Units are 10^{-19} cm^2 .
dose-coupling cal
Schwinger multich

^aValues are fro

^bValues are fro

^cData are from

^dNumbers are

^eValues are ob

re text.

^fData are from

^gData are fro

ower energies.
parameter calcul
B $^1\Sigma_g^+$ state cro
present cross se
times larger at
tions listed in T
Lin [1978] with
pear to be the cl
larger than exp
channel calculat
sections at low e
tal ones. Table
is more accurat
tion in the regi
It is instruct
with experim
approximation
The large diffe
components su

Maurice [1971]

Table 8. Comparison of H₂ Ly Cross Sections.

Present Study	P ^a	IP ^b	P ^c	IP ^d	CC ^e	DW ^f	Born ^g	Born ^h	SMC ⁱ
	E, eV	300 K	300 K	1000 K	1000 K				
15	91.3	389	93.8	394	...	105	375	360	141
20	199	449	202	457	...	309	530	523	266
25	255	527	259	537	431	412	573	564	...
30	285	563	289	572	...	446	577	569	400
35	301	574	304	582	567
40	308	571	311	579	...	493	551	543	...
45	310	560	313	568	532
50	308	547	312	554	471	484	513	506	...
60	301	515	304	523	...	449	477	470	...
70	291	...	294	445
75	286	...	289	...	409	...	430
80	281	457	284	463	417
100	262	408	264	414	358	...	370
150	225	...	227	290
200	198	...	200	240
300	160	...	161	181
400	134	...	135	147
500	115	...	116	125
600	101	...	102	110
700	90.7	...	91.5	97.7
800	82.3	...	83.0	88.3
900	75.4	...	76.1	80.8
1000	69.7	...	70.4	74.6
1100	64.9	...	65.5	69.4
1200	60.8	...	61.3	65.2
1300	57.2	...	57.7	62.0

Units are 10^{-19} cm^2 . Abbreviations are P for present experimental work; IP for impact-parameter calculation; CC for close-coupling calculation; DW for distorted wave Born closure calculation; Born for Born-approximation; and SMC for Schwinger multichannel calculation.

^aValues are from present experimental work.

^bValues are from impact-parameter calculation by Redmon et al. [1985].

^cData are from two state close-coupling calculation of Chung and Lin [1978].

^dNumbers are from L^2 distorted wave Born closure calculation by Fliflet and McKoy [1980].

^eValues are obtained in the present work by integrating generalized oscillator strength of Kolos et al. [1982a, b, 1983]; see text.

^fData are from Born calculation by Fliflet and McKoy [1980].

^gData are from Schwinger multichannel calculation by Gibson et al. [1987].

lower energies. For example, the semiclassical impact-parameter calculation by Redmon et al. [1985] yielded a B $^1\Sigma_u^+$ state cross section 2.3–1.6 times larger than the present cross section in the 20–100 eV region and 4.3 times larger at 15 eV. Among the calculated cross sections listed in Table 8, those calculated by Chung and Lin [1978] with the two-state close-coupling method appear to be the closest to our cross sections, 1.4–1.7 times larger than experiment. Overall, the Schwinger multichannel calculation by Gibson et al. [1987] yielded cross sections at low energy that are closest to the experimental ones. Table 8 also shows that the Born cross section is more accurate than the impact-parameter cross section in the region above 60 eV (see also Figure 4).

It is instructive to compare the Born cross section with experiment. In the low-energy region the Born approximation seriously overestimates the cross section. The large difference shows the importance of non-Born components such as polarization and exchange interac-

tions, as well as coupling among various states in the low-energy region. The contributions from interactions not included in the Born theory decrease with increasing energy, and therefore the differences between Born and experimental cross sections also decrease. However, it must be emphasized that the contributions from the non-Born components are still important even at 1200 eV. For example, the Born cross section calculated from the data of Kolos et al. [1982a, b, 1983] is ~16% larger than the experimental cross section at 1250 eV. (It should be noted that experimental cross sections listed in Table 8 are obtained using experimental threshold energies and oscillator strengths calculated by Abgrall et al. 1987, 1993a, b, c. The Abgrall oscillator strength fully account for the perturbations between the B $^1\Sigma_u^+$ and C $^1\Pi_u^+$ states and J dependence of electronic transition dipole matrix element. However, Born cross sections listed in Table 8 are obtained for hypothetical transitions between $J_i = 0$ and $J_f = 0$ with

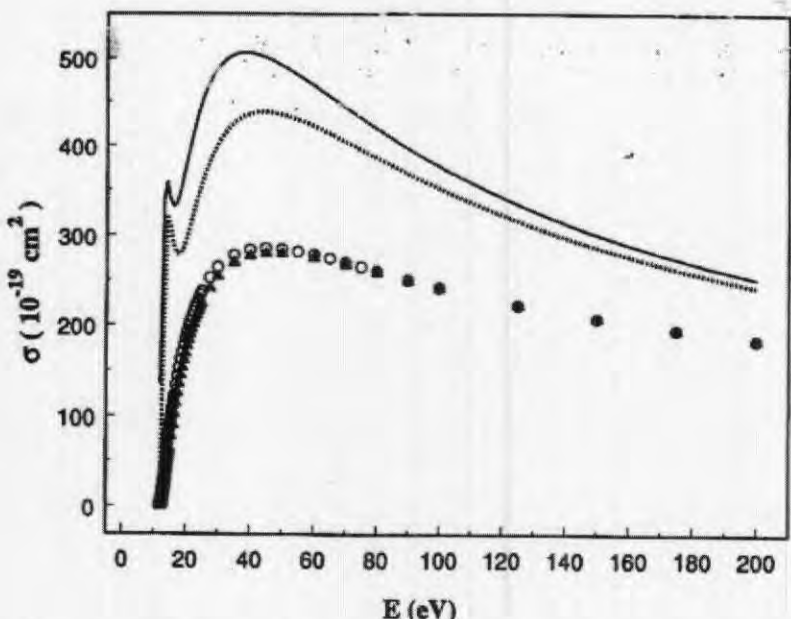


Figure 4. Comparison between theoretical and experimental cross sections. The calculated cross sections of the Ly (solid line) and W (dotted line) band system are from the refined impact-parameter calculation of *Celiberto and Rescigno* [1993]. The experimental cross sections for Ly (open circles) and W (solid triangles) bands are generated with the present shape function and by assuming temperature $T = 10$ K.

slightly different oscillator strength. The 16% difference reported here is obtained when both cross sections are computed from the same oscillator strengths and threshold energies.) The difference indicates that the contribution from the non-Born interactions is not negligible (that is, the Born limit is not reached) unless excitation energy reaches a few keV (> 4 keV). The indication is consistent with the recent results in atomic hydrogen of James *et al.* [1997].

Celiberto and Rescigno [1993] have calculated excitation cross sections of H₂ Ly and W bands via different vibrational levels of the X state with the impact-parameter method. In their original calculation the vibrational levels of the B ¹ Σ_u^+ and C ¹ Π_u states were treated as if they were degenerate. Subsequently, Celiberto and Rescigno refined the cross-section calculation by considering differences in the energy of the vibrational levels of the B ¹ Σ_u^+ and C ¹ Π_u states. Figure 4 compares the refined H₂ Ly and W excitation cross section from the v_i = 0 levels of the X state with the present cross section. Since rotational motion was not considered in the calculation by Celiberto and Rescigno [1993], the present B ¹ Σ_u^+ and C ¹ Π_u cross sections are generated for comparison by assuming T = 10 K, in which excitation from the J_i = 0 level of the X state is dominant.

There are several apparent differences between the calculated and present cross sections shown in Figure 4. First, the calculated $B\ ^1\Sigma_u^+$ and $C\ ^1\Pi_u$ state cross sections are ~95% and 65% larger than the experimentally measured $B\ ^1\Sigma_u^+$ and $C\ ^1\Pi_u$ state cross sections, respectively. In addition, the calculated $B\ ^1\Sigma_u^+$ and $C\ ^1\Pi_u$

$^1\Pi_u$ state cross sections have sharp peaks in the 13–17 eV regions, while the present cross sections are smooth and do not have any similar sharp peaks. Furthermore, Celiberto and Rescigno [1993] predicted that the $B\ ^1\Sigma^+$ state cross section is $\sim 5\text{--}15\%$ larger than the $C\ ^1\Pi_u$ state. This study, however, indicates that the $B\ ^1\Sigma^+$ state cross section is only slightly larger (5%) than the $C\ ^1\Pi_u$ state cross section. Finally, the calculated cross sections rise much faster than the measured cross section in the threshold region.

Since all the theoretical cross sections, when normalized to common oscillator strengths, should converge to the same Born cross section at high energy, the differences between various cross sections in the low or medium energy region must be caused by the difference in the shapes of the excitation functions.

5.6. Dissociative Excitation of H Ly α at 100 eV

The cross section values at 100 eV for (1c) obtained in the more recent accurate work are shown in Table 9. Several aspects of these results should be considered in making judgments on the relative merits of these results.

In addition to the method employed here, the H Ly α emission cross section can also be obtained from the intensity of the whole H₂ Ly and W band systems of H₂. Using the *Allison and Dalgarno* [1970] band oscillator strength partitioned by Hönl-London factors, SAH determined the H Ly α /H₂ Ly band and H Ly α /H₂ W band cross-section ratio to be 0.293 and 0.306, respectively.

Table 2. Cross

Van Zyl et al.
Woolsey et al.
Ligtkenberg et al.
De Heer and C
Shemansky et al.
This study

Units are 10⁻³
Data are from
Data are re-

tively, at 100 eV the state cross section is 1.1 cm^2 (at 300 eV) and $7.67 \times 10^{-18} \text{ cm}^2$ (at 10 eV). SAH did not observe the $B^1\Sigma_u^+$ and $C^1\Pi_g$ states in the 1-2 eV emission cross sections. The appropriate bound state cross sections are approximately canceled with (7.16 \pm 0.05) cm^2 relative line intensity.

The H Ly α transition energy (Table 9). van De Heer and et al. [1985a] made a measurement of (7.22 ± 1.1) eV from H and He II using synchrotron radiation and obtained a value of (7.16 ± 0.5) eV. The values determined by van De Heer and et al. [1985] are in agreement with the present measurement of (7.16 ± 0.5) eV. The H β cross section is given as 7.53×10^{-18} cm 2 sr $^{-1}$ eV $^{-1}$ by SAH. The H γ cross section is given by van De Heer and Carrière [1985] as 1.0×10^{-18} cm 2 sr $^{-1}$ eV $^{-1}$. The H δ cross section is given by van De Heer and et al. [1985] as 1.0×10^{-18} cm 2 sr $^{-1}$ eV $^{-1}$. The H ϵ cross section is given by van De Heer and et al. [1985] as 1.0×10^{-18} cm 2 sr $^{-1}$ eV $^{-1}$. The H ζ cross section is given by van De Heer and et al. [1985] as 1.0×10^{-18} cm 2 sr $^{-1}$ eV $^{-1}$.

Table 9. Cross Section for Dissociative Excitation of H Ly α at 100 eV

Source	σ^a	σ^b
Van Zyl et al. [1985]	7.22 ± 1.30	...
Woolsey et al. [1986]	7.13 ± 0.59	6.81 ± 0.59
Ligtenberg et al. [1985]	6.57 ± 0.53	...
De Heer and Carrière [1971]	10.3 ± 2.1	7.37 ± 1.2
Shemansky et al. [1985a]	8.18 ± 1.2	7.53
This study	7.16 ± 0.95	...

Units are 10^{-18} cm^2 .

^aData are from original reports.

^bData are revised in this work; see text.

tively, at 100 eV. Using the present $B^1\Sigma_u^+$ and $C^1\Pi_u$ state cross sections, 2.618×10^{-17} and $2.413 \times 10^{-17} \text{ cm}^2$ (at 300 K), we obtain the H Ly α cross section 7.67×10^{-18} and $7.38 \times 10^{-18} \text{ cm}^2$, respectively. Since SAH did not consider the effect of perturbation on the $B^1\Sigma_u^+$ and $C^1\Pi_u^+$ state cross sections, an averaged 100 eV mission cross section, $7.53 \times 10^{-18} \text{ cm}^2$, is more appropriate because the effect of perturbation approximately cancels out. The averaged number agrees well with $(7.16 \pm 0.95) \times 10^{-18} \text{ cm}^2$ determined with the relative line intensity measurements.

The H Ly α emission cross section at 100 eV excitation energy has been measured by many authors, including Van Zyl et al. [1985], Ligtenberg et al. [1985], De Heer and Carrière [1971], and Woolsey et al. [1986] (Table 9). van der Burgt et al. [1989] and Shemansky et al. [1985a] have reviewed many early experimental measurements. Van Zyl et al. [1985] obtained a value of $(7.22 \pm 1.30) \times 10^{-18} \text{ cm}^2$ by measuring H Ly α from H and Ne collision, while Ligtenberg et al. [1985], using synchrotron radiation as a calibration standard, obtained a value of $(6.57 \pm 0.53) \times 10^{-18} \text{ cm}^2$. The values determined by Van Zyl et al. [1985] and Ligtenberg et al. [1985] agree very well with the present measurement of $(7.16 \pm 0.95) \times 10^{-18} \text{ cm}^2$ or with the value $7.53 \times 10^{-18} \text{ cm}^2$ based on the cross-section ratio of SAH. The H Ly α emission cross section of De Heer and Carrière [1971], however, needs to be corrected. De Heer and Carrière [1971] measured the intensities of Ly α region relative to the intensities of H₂ W(3,7) band emissions. Using their H₂ W(3,7) band emission cross section at 100 eV, they determined the H Ly α emission cross section to be $(10.3 \pm 2.1) \times 10^{-18} \text{ cm}^2$. However, as Table 7 shows, the De Heer and Carrière [1971] C $^1\Pi_u$ state cross section at 100 eV is ~33% larger than the present cross section. If the present cross section were used, the H Ly α emission cross section would have been $(10.3 \pm 2.1) \times 10^{-18} \times 241/320$ or $(7.76 \pm 1.6) \times 10^{-18} \text{ cm}^2$. Moreover, the spectral resolution of De Heer and Carrière [1971] was not high enough to resolve the H₂ W(2,6) band emission from the H Ly α emission. While the detailed spectral resolution was not given, De Heer and Carrière [1971] estimated that the H₂ W(2,6) band contributed about or less than 5%

of the total intensity over the selected H Ly α region. If one assumes the contribution of molecular emission lines in the H Ly α region is 5%, the H Ly α emission cross section obtained by De Heer and Carrière [1971] should be revised as $(7.37 \pm 1.2) \times 10^{-18} \text{ cm}^2$, a result which is very close to the $(7.16 \pm 0.95) \times 10^{-18} \text{ cm}^2$ of the present experiment, or $7.53 \times 10^{-18} \text{ cm}^2$ based on the cross section-ratio of SAH. The H Ly α emission cross section from (1c) and (1d) at 100 eV obtained in this study is also in good agreement with the $(7.13 \pm 0.59) \times 10^{-18} \text{ cm}^2$ cross section reported by Woolsey et al. [1986]. The cross section of Woolsey et al. [1986] was obtained by measuring relative intensities of H Ly α emission resulting from 100 eV excitation of ground state H₂ and from H(1s) and by using the apparent absolute excitation cross section of H(1s) of Long et al. [1968] and Kauppila et al. [1971]. The apparent excitation cross section of H(1s) 100 eV used by Woolsey et al. [1986] is $(6.0 \pm 0.2) \times 10^{-18} \text{ cm}^2$. A more recent benchmark experimental study of James et al. [1997] has recommended $5.44 \times 10^{-18} \text{ cm}^2$ as the cross section for direct H(1s) \rightarrow H(2p) excitation at 100 eV. The cascade excitation contribution to the formation of H(2p) can be estimated to be $0.29 \times 10^{-18} \text{ cm}^2$ at 100 eV. Thus the 100 eV apparent cross section, based on the work of James et al. [1997], is $5.73 \times 10^{-18} \text{ cm}^2$. If the apparent cross section of James et al. [1997] is used, the Woolsey et al. [1986] H Ly α emission cross section resulting from (1c) and (1d) at 100 eV is revised as $(6.81 \pm 0.59) \times 10^{-18} \text{ cm}^2$, which is very close to the value $(7.16 \pm 0.95) \times 10^{-18} \text{ cm}^2$ of this work.

The accuracy of the C $^1\Pi_u$ state cross section near the 100 eV region can be examined by comparing the present H Ly α emission cross section with those determined by other work. As stated earlier, the H Ly α emission cross section from (1c) and (1d) is obtained by assuming that the uncertainty in the C $^1\Pi_u$ state cross section at 100 eV is negligible. The fact, however, that the present H Ly α emission cross section agrees very well with the independently determined results of Van Zyl et al. [1985], Ligtenberg et al. [1985], and Woolsey et al. [1986] suggests that the uncertainty in the present B $^1\Sigma_u^+$ and C $^1\Pi_u$ state cross sections of molecular hydrogen near the 100 eV region is, at most, 15%.

6. Conclusions

Analysis of H₂ Ly and W electron-impact-induced emission indicates that cross-section shape functions of the two systems are the same within experimental error. The energy dependence of the B $^1\Sigma_u^+$ and C $^1\Pi_u$ state excitation cross sections are therefore essentially identical when excitation energy is expressed in terms of threshold energy units. We have obtained excitation functions by merging the present data truncated at 250 eV with data of De Heer and Carrière [1971] from 100 to 3000 eV. Table 1 lists the parameters that define the collision strength shape function for direct excitation, (4a)-(4c).

The present H₂ B $^1\Sigma_u^+$ and C $^1\Pi_u$ state cross sections are significantly improved over those obtained by SAH.

High-resolution spectra make it possible to measure the energy dependence of the cross sections more precisely than SAH. The more accurate excitation shape function of the present study has removed a large relative error between the B¹ Σ_u^+ and C¹ Π_u states in the low- and medium-energy regions. Furthermore, application of accurate line oscillator strengths calculated by Abgrall *et al.* [1987, 1993a, b, c] and Abgrall and Roueff [1989] enables a full account of perturbations and rotational dependence of the transition dipole matrix elements, as well as a calculation of the cross section at the rotational level.

Our H₂ B¹ Σ_u^+ state cross section is in good agreement with the B¹ Σ_u^+ state cross section determined by Khakoo and Trajmar [1986]. However, the present C¹ Π_u state cross section is significantly larger than the C¹ Π_u state value of Khakoo and Trajmar [1986]. The analysis suggests that the experimental uncertainty of Khakoo and Trajmar [1986] is likely larger than reported. The present H₂ C¹ Π_u state cross sections are 5–11% smaller than the rescaled C¹ Π_u state cross section of De Heer and Carrière [1971] in the 50–100 eV region.

We have determined the dissociatively excited H Ly α emission cross section at 100 eV from emission measurements relative to H₂ band lines at high resolution. The present H Ly α emission cross section is in good agreement with the cross sections obtained by Van Zyl *et al.* [1985], Ligtenberg *et al.* [1985], and Woolsey *et al.* [1986] and consistent with the corrected H Ly α emission cross sections of De Heer and Carrière [1971] and SAH. The good agreement in the H Ly α emission cross section (1c) and (1d) with other independent results gives greater confidence in the accuracy of the present absolute C¹ Π_u (and by inference, B¹ Σ_u^+) state cross section near 100 eV.

A comparison of the present H₂ B¹ Σ_u^+ and C¹ Π_u state cross sections with theoretical cross sections indicates that the theoretical cross sections are larger than experiment by a factor of ~2 in the low- and medium-energy regions. As all the observed and calculated cross sections are normalized to the same oscillator strength at high energy (Born limit), large low-energy differences suggest the theoretical calculations do not accurately account for coupling and momentum transfer effects. It appears that H and H₂ present an extreme in the magnitude of coupling and momentum transfer effects causing deviation from uncoupled Born theory into the high-energy region [see James *et al.*, 1997]. The effect of these terms is far less severe in other species, helium, for example [Shemansky *et al.*, 1985b].

Experimental errors are estimated to be 15%–25% when the excitation energy is between 20 and 500 eV, and 7%–15% above 500 eV. The finite energy width of the electron gun is expected to cause increased uncertainty in the threshold energy region, and errors can be as large as ~30% in the 14–20 eV region. The primary source of the error is secondary electrons trapped by the magnetically collimated electron gun, although uncertainties in the electron energy scale, finite electron

energy width, and drifting of electron gun parameters also contribute.

The present study deals only with the direct electron excitation channels for H₂. Other known channels are electron attachment resonance and cascade from the E, F¹ Σ_g^+ state. Resonance excitation primarily enhances the low vibrational levels of the B¹ Σ_u^+ and C¹ Π_u states. The resonance contribution is negligible at impact energy >16 eV. The E, F¹ Σ_g^+ – B¹ Σ_u^+ cascade excitation takes place with an electric dipole forbidden transition from the X state to the E, F state and subsequent transition to the B state. Cascade excitation enhances the population of the $v_f = 0$ –4 levels of the B¹ Σ_u^+ state. Ajello *et al.* [1984] and SAH have estimated the contribution of cascade in the 100–300 eV region to be ~14%–10% of the direct excitation cross section. A reexamination of E, F¹ Σ_g^+ – B¹ Σ_u^+ cascade indicates the earlier (SAH) estimate of cross-section shape is severely affected by secondary electrons. Work is currently underway to refine the E, F excitation function.

The effect of the present results on previous work in the interpretation of planetary atmosphere emission is extensive but difficult to assess accurately without careful reanalysis. Most of the published work, including recent efforts, did not consider the effect of electron energy distribution on the relative line or band intensities. We do not mean to infer that previous analyses were basically correct; they are most likely tainted by secondary electron temperature effects that were never considered. The most recent work on Galileo auroral observations at Jupiter utilized the cross sections in this study [Pryor *et al.*, 1998; Ajello *et al.*, 1998]. These results indicate that electron characteristic temperatures are low (for example, T_e ~ 27 eV) in auroral excitation. The so called "color ratios", utilized in earlier work as indicating the level of involvement of CH₄ in radiation transmission [cf. Yung *et al.*, 1982; Prang *et al.*, 1995], are most likely tainted by electron temperature effects. The electron temperature estimates in Saturn auroral and Jupiter dayglow observations [Shemansky and Ajello, 1983; Shemansky, 1985] are too high by ~30% or more, based on the current cross sections. This assessment is by no means comprehensive, and there are a large number of affected published works that are not mentioned here.

Acknowledgments. We would like to thank R. Celiberto and T.N. Resicigno for providing the refined numerical values of their impact-parameter cross-section calculation. We would also like to thank J.-Y. Roncin and F. Launay for providing experimentally determined energy levels of the B¹ Σ_u^+ and C¹ Π_u states and H. Abgrall and E. Roueff for their valuable comments and suggestions. The present work was carried out at the Jet Propulsion Laboratory and the University of Southern California. We wish to acknowledge grant support from the National Science Foundation (ATM-9320589) and NASA (NAG5-4591) to the University of Southern California, NASA Planetary Atmospheres, Astronomy/Astrophysics and Space Physics Offices (NAGW-3905), and Air Force Office of Scientific Research (AFOSR) to the Jet Propulsion Laboratory. Part of the work reported in the present paper was performed while X. Liu and S. M.

Ahmed held N
at the Jet Pro
The Editor
writing this pa

Reference

- Abgrall, H., and transiti... Werner 328, 1989.
- Abgrall, H., F... Werner trum of H₂, 1993a.
- Abgrall, H., L. Subtil, T... hydrogen, 1993b.
- Abgrall, H., L. Subtil, T... hydrogen, 1993c.
- Abgrall, H., L. Subtil, T... hydrogen, 1994.
- Ajello, J. M., Studies of series of H₂ b 1984.
- Ajello, J. M., of Jupiter 1998.
- Allison, A. C and transi... systems of Tables, 1, 133–141, 1993.
- Arrighini, G. Marinelli, 1993.
- Celiberto, R. impact ex... quantum B¹ Σ_u^+ and 1993.
- Chan, W. F. oscillator photoabsor... Werner ba Chung, S., a method to of H₂ by 1978.
- Dabrowski, J. Phys., De Heer, F. band syst... Dressler, K. ments for J. Chem., Fliflet, A. V. cross sect of H₂ by 1863–187 Fujimoto, ciation r J. Appl.

parameters direct electron channels cascade from primarily en- $^1\Sigma_u^+$ and C $^1\Sigma_u^+$ negligible at $^1\Sigma_u^+$ cascade level forbidded state and sub- e excitation levels of the B Σ_u^+ estimated 0 eV region cross section. cascade indi- cation shape Work is cur- in function. Previous work re emission ally without work, includ- of electron band intensities analyses tained by were never leto auroral ions in this . These re- mperatures lar excita- l in earlier of CH₄ in 32; Prangé- ctron tes- stimates [Sh- i] are too cross se- prehensive, shed works

held National Research Council Associate positions at Jet Propulsion Laboratory. The Editor thanks the referees for their assistance in evaluating this paper.

References

- Abgrall, H., and E. Roueff, Wavelengths, oscillator-strength and transition probabilities of the H₂ molecule for Lyman and Werner systems, *Astron. Astrophys. Suppl.*, **79**, 313-328, 1989.
- Abgrall, H., F. Launay, E. Roueff, and J. Y. Roncin, Effect of rotational coupling on emission probabilities of Lyman and Werner band systems of the vacuum ultraviolet spectrum of H₂, *J. Chem. Phys.*, **87**, 2036-2044, 1987.
- Abgrall, H., E. Roueff, F. Launay, J. Y. Roncin, and J. L. Subtil, Table of the Lyman band system of molecular hydrogen, *Astron. Astrophys. Suppl. Ser.*, **101**, 273-321, 1993a.
- Abgrall, H., E. Roueff, F. Launay, J. Y. Roncin, and J. L. Subtil, Table of the Werner band system of molecular hydrogen, *Astron. Astrophys. Suppl. Ser.*, **101**, 323-362, 1993b.
- Abgrall, H., E. Roueff, F. Launay, J. Y. Roncin, and J. L. Subtil, The Lyman and Werner band systems of molecular hydrogen, *J. Mol. Spectrosc.*, **157**, 512-523, 1993c.
- Ajello, J. M., D. E. Shemansky, T. L. Kwok, and Y. L. Yung, Studies of extreme-ultraviolet emission from Rydberg series of H₂ by electron impact, *Phys. Rev. A*, **29**, 636-653, 1984.
- Ajello, J. M., et al., Galileo orbiter ultraviolet observations of Jupiter aurora, *J. Geophys. Res.*, **103**, 20125-20148, 1998.
- Allison, A. C., and A. Dalgarno, Band oscillator strengths and transition probabilities for the Lyman and Werner systems of H₂ and HD, and D₂, *At. Data Nucl. Data Tables*, **1**, 289-304, 1970.
- Arrighini, G. P., F. Boindi, C. Guidotti, A. Biagi, and F. Marinelli, Inelastic scattering of fast electrons from molecular systems, I., Hydrogen molecule, *Chem. Phys.*, **52**, 133-141, 1980.
- Celiberto, R., and T. N. Rescigno, Dependence of electron-impact excitation cross sections on the initial vibrational quantum number in H₂ and D₂ molecules: X $^1\Sigma_g^+$ \rightarrow B $^1\Sigma_u^+$ and X $^1\Sigma_g^+$ \rightarrow C $^1\Pi_u$, *Phys. Rev. A*, **47**, 1939-1945, 1993.
- Chan, W. F., G. Cooper, and C. E. Brion, Absolute optical oscillator strengths (11-20 eV) and transition moments for photoabsorption of molecular hydrogen in the Lyman and Werner bands, *Chem. Phys.*, **168**, 375-388, 1992.
- Chung, S., and C. C. Lin, Application of the close-coupling method to excitation of electronic states and dissociation of H₂ by electron impact, *Phys. Rev. A*, **17**, 1874-1884, 1978.
- Dabrowski, I., The Lyman and Werner bands of H₂, *Can. J. Phys.*, **62**, 1639-1664, 1984.
- De Heer, F. J., and J. D. Carrière, Emission of the Werner band system and Lyman- α radiation for 0.05-6-keV electrons in H₂, *J. Chem. Phys.*, **55**, 3829-3835, 1971.
- Dressler, K., and L. Wolniewicz, Electronic transition moments for the Lyman and Werner bands of the H₂ molecule, *J. Chem. Phys.*, **82**, 4720-4721, 1985.
- Fliflet, A. W., and V. McKoy, Distorted-wave-approximation cross sections for excitation of the b $^3\Sigma_u^+$ and B $^1\Sigma_u^+$ states of H₂ by low-energy-electron impact, *Phys. Rev. A*, **21**, 1863-1875, 1980.
- Fujimoto, T., and K. Sawada, Effective ionization and dissociation rate coefficients of molecular-hydrogen in plasma, *J. Appl. Phys.*, **78**, 2913-2924, 1995.
- Gibson, T. L., M. A. P. Lima, V. McKoy, and W. M. Huo, Application of the Schrödinger multichannel formulation to electron-impact excitation of the B $^1\Sigma_u^+$ state of H₂, *Phys. Rev. A*, **35**, 2473-2478, 1987.
- Hiskes, J. R., Atomic processes, cross-sections, and reaction-rates necessary for modeling hydrogen negative-ion sources and identification of optimum H-current densities, *Rev. Sci. Instrum.*, **63**, 2702-2704, 1992.
- Hiskes, J. R., Optimum extracted H- and D-current densities from gas-pressure-limited high-power hydrogen-deuterium tandem ion sources, *Rev. Sci. Instrum.*, **65**, 1219-1221, 1994.
- Hiskes, J. R., Molecular Rydberg states in hydrogen negative-ion discharges, *Appl. Phys. Lett.*, **69**, 755-757, 1996.
- Hiskes, J. R., A. M. Karo, and P. A. Willmann, Optimum extracted negative-ion current densities from tandem high-density systems, *J. Appl. Phys.*, **58**, 1759-1764, 1985.
- James, G. K., J. A. Slevin, D. E. Shemansky, J. W. McConkey, I. Bray, D. Dzicsek, I. Kanik, and J. M. Ajello, Optical excitation function of H (1s-2p) produced by electron impact from threshold to 1.8 keV, *Phys. Rev. A*, **55**, 1069-1087, 1997.
- Kauppila, W. E., P. J. O. Teubner, W. L. Fite, and R. J. Girnus, Lyman-alpha emission induced by the collision of electron with molecular hydrogen, *J. Chem. Phys.*, **55**, 1670-1672, 1971.
- Khakoo, M. A., and S. Trajmar, Electron impact excitation of the a $^3\Sigma_g^+$, B $^1\Sigma_u^+$, c $^3\Pi_u$, and C $^1\Pi_u$ of H₂, *Phys. Rev. A*, **34**, 146-156, 1986.
- Kolos, W., H. J. Monkhorst, and K. Szalewicz, Energy unresolved differential cross section for electron scattering by H₂, *J. Chem. Phys.*, **77**, 1323-1334, 1982a.
- Kolos, W., H. J. Monkhorst, and K. Szalewicz, Inelastic high-energy electron scattering from a hydrogen molecule, I., X-B and X-E transitions, *J. Chem. Phys.*, **77**, 1335-1344, 1982b.
- Kolos, W., H. J. Monkhorst, and K. Szalewicz, Generalized oscillator strengths for X-B transitions in the hydrogen molecule, *At. Data Nucl. Data Tables*, **28**, 239-263, 1983.
- Lichtenberg, R. G., A. McPherson, N. Rouze, W. Westerveld, and J. S. Risley, *Proceedings of the XIVth International Conference on Physics of Electronic and Atomic Collisions*, 276pp Am. Inst. of Phys., College Park, Md., 1985.
- Liu, X., S. M. Ahmed, R. A. Multari, G. K. James, and J. M. Ajello, High-resolution electron-impact study of the far-ultraviolet emission spectrum of molecular hydrogen, *Astrophys. J. Suppl. Ser.*, **101**, 375-399, 1995.
- Long, R. L., D. M. Cox, and S. J. Smith, Electron Impact Excitation of Hydrogen Lyman- α Radiation, *J. Res. Natl. Bur. Stand. U. S.*, **72**, 521-535, 1968.
- Moustafa-Moussa, H. R., F. J. DeHeer, and J. Schutten, Excitation of helium by 0.05-6 keV electrons and polarization of the resulting radiation, *Physica*, **40**, 517, 1969.
- Prangé, R., D. Rego, and J. C. Gerard, Auroral Lyman α and H₂ from the giant planets, 2., Effect of the anisotropy of the precipitating particles on the interpretation of "color ratio", *J. Geophys. Res.*, **100**, 7513-7521, 1995.
- Pryor, W. R., et al., Galileo ultraviolet spectrometer observations of Jupiter's auroral spectrum from 1600-3200 Å, *J. Geophys. Res.*, **103**, 20149-20158, 1998.
- Redmon, M. J., B. C. Garrett, L. T. Redmon, and C. W. McCurdy, Improved impact-parameter method for electronic excitation and dissociation of diatomic molecules by electron impact, *Phys. Rev. A*, **32**, 3354-3365, 1985.
- Roncin, J. Y., and F. Launay, *Atlas of the Vacuum-Ultraviolet Emission Spectrum of Molecular Hydrogen*, Am. Chem. Soc., Washington, D. C., 1994.
- Schram, B., F. DeHeer, M. Vander Wiel, and J. Kistemaker,

- Ionization cross sections for electrons (0.6–220 keV) in noble and diatomic gases, *J. Phys.*, **31**, 94–112, 1965.
- Shemansky, D. E., An explanation for the H Ly_α longitudinal asymmetry in the equatorial spectrum of Jupiter: An outcrop of paradoxical energy deposition in the exosphere, *J. Geophys. Res.*, **90**, 2673–2694, 1985.
- Shemansky, D. E., and J. M. Ajello, The Saturn spectrum in the EUV - electron excited hydrogen, *J. Geophys. Res.*, **88**, 459–464, 1983.
- Shemansky, D. E., J. M. Ajello, and D. T. Hall, Electron impact excitation of H₂: Rydberg band systems and benchmark dissociative cross section for H Lyman alpha, *Astrophys. J.*, **296**, 765–773, 1985a.
- Shemansky, D. E., J. M. Ajello, D. T. Hall, and B. Franklin, Vacuum ultraviolet studies of electron impact of helium: Excitation of He *nℓ P°* Rydberg series and ionization-excitation of He⁺ *nℓ* Rydberg series, *Astrophys. J.*, **296**, 774–783, 1985b.
- Srivastava, S. K., and S. Jensen, Experimental differential and integral electron impact cross sections for the B $^1\Sigma_u^+$ state of H₂ in the intermediate energy region, *J. Phys. B At. Mol. Phys.*, **10**, 3341–3346, 1977.
- Szalewicz, K., W. Kolos, H. J. Monkhorst, and C. Jackson, Effect of vibrations on the energy unresolved electron scattering by H₂ and D₂, *J. Chem. Phys.*, **80**, 1435–1439, 1984.
- Trajmar, S., D. F. Register, and A. Chutjian, Electron scattering by molecules, II., Experimental method and data, *Phys. Rep.*, **97**, 219–356, 1983.
- van der Bergt, P. J. M., W. B. Westerveld, and J. S. Risley, Photoemission cross sections for atomic transitions in the extreme ultraviolet due to electron collisions with atoms and molecules, *J. Phys. Chem. Ref. Data*, **18**, 1757–1805, 1989.
- Van Zyl, B., M. W. Gealy, and H. Neumann, Excitation of low-energy H atoms in H + Ne collisions, *Phys. Rev. A*, **31**, 2922–2931, 1985.
- Woolsey, J. M., J. L. Forand, and J. W. McConkey, Lyman α revisited, *J. Phys. B At. Mol. Phys.*, **19**, L493–L497, 1986.
- Yung, Y. L., G. R. Gladstone, K. M. Chang, J. M. Ajello, and S. K. Srivastava, H₂ fluorescence spectrum from 1200 to 1700 Å by electron impact: Laboratory study and application to Jovian aurora, *Astrophys. J. Lett.*, **254**, L65–L68, 1982.
- S. M. Ahmed, Institute for Plasma Research, Bhat, Gandhinagar, 382, 428, India. (email: ahmed@plasma.ernet.in)
- J. M. Ajello and G. K. James, Jet Propulsion Laboratory, 4800 Oak Grove Drive, Pasadena, CA 91109. (email: gjames@jpluvs.jpl.nasa.gov; jajello@jpluvs.jpl.nasa.gov)
- X. Liu and D. E. Shemansky, Department of Aerospace Engineering, University of Southern California, Los Angeles, CA 90089. (email: xliu@jpluvs.jpl.nasa.gov; dongs@hippolyta.usc.edu)

(Received April 10, 1998; revised July 9, 1998; accepted August 14, 1998.)

Comment
variations'
Rowell, A.

Chaman-Lal
Beneda, Maryland

1. Introduction

Willard et al.
Coupled Thermos
that the semiannual
the F2 layer is ca
the altitude of the
be justified as it
The thrust of their
unique to the F2
the UV/EUV sol
appear to be justif

The purpose of
authors an altern
addition to the UV
of the ionosphere
signatures to the
semiannual variati
corner stone in
physically meanin
critical frequency
cycle 19 from 19%
percent of the pi
calculations are wi
We ascribe the F
monthly median vi
and covering all lo
activity, to the in
tem. Consequent
of the model seem
model. We hope
in the pursuit of
comments.

2. Semiannual

Cook [1967, 19
a semiannual varia
to the exosphere
observations, Peat.
reported similar s
density. We have

Copyright 1998 by t

Paper number 98J/
1148-0227/98/98JA